IAEA-TECDOC-1441

Effects of nickel on irradiation embrittlement of light water reactor pressure vessel steels

IAEA
International Atomic Energy Agency

June 2005

IAEA-TECDOC-1441

Effects of nickel on irradiation embrittlement of light water reactor pressure vessel steels

IAEA
International Atomic Energy Agency

June 2005

The originating Section of this publication in the IAEA was:

Nuclear Power Engineering Section
International Atomic Energy Agency
Wagramer Strasse 5
P.O. Box 100
A-1400 Vienna, Austria

EFFECTS OF NICKEL ON IRRADIATION EMBRITTLEMENT OF
LIGHT WATER REACTOR PRESSURE VESSEL STEELS
IAEA, VIENNA, 2005
IAEA-TECDOC-1441
ISBN 92–0–103305–2
ISSN 1011–4289

Printed by the IAEA in Austria
June 2005

FOREWORD

This TECDOC was developed under the IAEA Coordinated Research Project (CRP) entitled Effects of Nickel on Irradiation Embrittlement of Light Water Reactor Pressure Vessel (RPV) Steels. This CRP is the sixth in a series of CRPs to determine the influence of the mechanism and quantify the influence of nickel content on the deterioration of irradiation embrittlement of reactor pressure vessel steels of the Ni-Cr-Mo-V or Mn-Ni-Cr-Mo types. The scientific scope of the programme includes procurement of materials, determination of mechanical properties, irradiation and testing of specimens in power and/or test reactors, and microstructural characterization.

Eleven institutes from eight different countries and the European Union participated in this CRP and six institutes conducted the irradiation experiments of the CRP materials. In addition to the irradiation and testing of those materials, irradiation experiments of various national steels were also conducted. Moreover, some institutes performed microstructural investigations of both the CRP materials and national steels. This TECDOC presents and discusses all the results obtained and the analyses performed under the CRP. The results analysed are clear in showing the significantly higher radiation sensitivity of high nickel weld metal (1.7 wt%) compared with the lower nickel base metal (1.2 wt%). These results are supported by other similar results in the literature for both WWER-1000 RPV materials, pressurized water reactor (PWR) type materials, and model alloys.

Regardless of the increased sensitivity of WWER-1000 high nickel weld metal (1.7 wt%), the transition temperature shift for the WWER-1000 RPV design fluence is still below the curve predicted by the Russian code (standard for strength calculations of components and piping in NPPs – PNAE G 7-002-86). For higher fluence, no data were available and the results should not be extrapolated. Although manganese content was not incorporated directly in this CRP, results from tests of national steels demonstrated that, for a given high level of nickel in the material, and all other factors being equal, high manganese content leads to much greater irradiation-induced embrittlement than low manganese content for both WWER-1000 and PWR materials. Experimental results and microstructural investigations for a very high nickel steel (~3.5 wt%) have indicated that, when there is very little content manganese, the radiation sensitivity is very low, even for such a high nickel steel.

This TECDOC can be used by research institutes, utilities, vendor organizations, regulators, and others to gain a better understanding of the effects of nickel on irradiation embrittlement of LWR RPV steels. Special thanks are due to R. Nanstad of ORNL (USA), who chaired the meetings, and to M. Brumovský (Czech Republic), A. Kryukov (Russian Federation), L. Debarberis (EU/JRC), and W. Server (USA) who, along with R. Nanstad, greatly contributed to the report. The IAEA officer responsible for this publication was Ki Sig Kang of the Division of Nuclear Power.

EDITORIAL NOTE

The use of particular designations of countries or territories does not imply any judgement by the publisher, the IAEA, as to the legal status of such countries or territories, of their authorities and institutions or of the delimitation of their boundaries.

The mention of names of specific companies or products (whether or not indicated as registered) does not imply any intention to infringe proprietary rights, nor should it be construed as an endorsement or recommendation on the part of the IAEA.

CONTENTS

1. INTRODUCTION

1.1. BACKGROUND

In most cases, the understanding of irradiation embrittlement behaviour of low alloy steels is based on the measurement of mechanical property changes (Charpy V-notch transition temperatures or yield strength increases) for steels that have been irradiated under a range of different conditions (neutron fluence/flux and temperature). Based on these mechanical test data alone, it often is not possible to explain observed results for these steels with respect to sometimes apparently conflicting data from other sources. However, by understanding the mechanism of irradiation damage in these materials, it is possible to address key issues that mechanical testing alone cannot explain. One germane example is the role of Ni as an alloying element in creating damage under irradiation conditions.

Although nickel is added to RPV steels to increase its hardenability and decrease the ductile-brittle transition temperature, it is generally accepted that the presence of nickel in reactor pressure vessel (RPV) steels increases its sensitivity to neutron induced embrittlement even at low phosphorus and copper concentrations. The mechanisms controlling the damage process are not well understood, although microstructural studies of irradiated RPV steels have shown clear evidence of nickel presence in irradiation-induced copper enriched precipitates, a copper-nickel synergistic effect and, more recently, a nickel-manganese synergistic effect.

However, there is only a limited quantity of data on neutron embrittlement of WWER-1000 steels (Ni-Cr-Mo-V) with high nickel content. Because of the significance of transition temperature shift predictions for WWER-1000 RPV integrity assessments, it is of great importance to investigate neutron embrittlement of light-water RPV steels containing high nickel contents, especially weld metals, including those typical of pressurized water reactor (PWR) RPVs (Mn-Ni-Cr-Mo). The improved prediction of transition temperature shifts would increase the reliability of both WWER-1000 and PWR RPV integrity assessments.

There are published data that demonstrate significant degraded behaviour of reactor pressure vessel steels with elevated levels of Ni and a discussion of these results is presented in Chapter 6. The discussion includes research results and surveillance data from WWER-1000 steels, PWR steels, and model alloys. Some of the these findings have led to a negative perception in the nuclear industry for the use of high Ni steels in reactor applications. In this regard, data for a very high nickel PWR steel (~3.3 mass %) are discussed in Chapter 5 that may mitigate such concern. To explain such effects, the mechanisms by which irradiation embrittlement occurs must be understood and, to reach such understanding, the synergistic effects of the various chemical constituents in the steels must be quantified more explicitly.

To quantify these effects, the irradiation-induced physical changes in the microstructures of the steels can be identified using state-of-the-art analytical techniques and these observations can be correlated with the observed changes in mechanical properties. Chapter 6 provides a discussion of the microstructural investigations conducted as part of the IAEA Coordinated Research Project (CRP). With understanding of the effects of irradiation on the microstructure and the mechanical properties, it is possible to describe the irradiation embrittlement process and develop physically-based models that can be used to more accurately predict embrittlement.

1.2. GOAL, OBJECTIVES AND SCOPE

The stated objective of the CRP is: "To determine the mechanism for and quantify the nickel content on the deteriorating effect in radiation embrittlement of reactor pressure vessel steels of Ni-Cr-Mo-V or Mn-Ni-Cr-Mo types." The scientific scope of the program includes procurement of materials, determination of mechanical properties, irradiation and testing of specimens in power and/or test reactors, and microstructural characterization. As a result of the inclusion of irradiation experiments in the CRP, the duration of the program was stated as "3 years as minimum."

The scope of the CRP includes the following:

- Analysis of mechanical properties and microstructure of materials in the as received state:
  - Tensile testing;
  - Impact testing of Charpy V-notch specimens;
  - Hardness and microhardness measurements;
  - Microstructural and fractographic investigations.
- Irradiation conditions for the participants' irradiation experiments.
- Analysis of mechanical properties and microstructural examination of materials in the post irradiation condition (same properties as listed above for the as received state).
- Analysis of the combined results in the as-received and irradiated conditions.
- Derivation of the relationship between the transition temperature shift dependence on neutron fluence taking into account nickel content.
- Results of tests and analyses with national steels.
- Recommendations for further research on the effects of nickel on irradiation-induced embrittlement mechanisms in RPV steels.

Thus, the goal of this CRP is to provide information based on the results obtained that will allow for improved understanding of the effects of nickel on light-water RPV embrittlement that will lead to the development of improved predictive techniques. A list of final reports from the participants is provided in the Appendix.

1.3. CONTRIBUTIONS OF INDIVIDUAL ORGANIZATIONS

The countries and laboratories involved in the CRP are identified in Table 1.1. The designation code for each participating organization is also indicated along with the type of specimen(s) and material(s) tested.

Table 1.1. Countries/organizations participating in the CRP and final contributions

Country/ Organization	Code	CRP Material Charpy Tests		National material(s) tested	Microstructure analysis
		Base metal	Weld metal		
Bulgaria-Bulgarian Academy of Sciences Institute of Metal Science	BUL	No	Yes	No	Yes
Czech Republic – NRI	NRI	Yes	Yes	No	No
Hungary – KFK Atomic Energy Research Institute	HUN	Yes	Yes	No	No
India – Bhabha Atomic Research Centre	IND	Yes[a]	Yes[a]	No	No
EC Joint Research Centre – Institute for Energy	JRC	Yes[a]	Yes[a]	Yes	No
Russia – RRC Kurchatov Institute	KUR	Yes	Yes	Yes	No
Russia – Prometey	PRO	Yes	Yes	Yes	No
Slovakia – Slovak University of Technology	SLO	No	No	No	Yes
Ukraine – National Academy of Sciences	UKR	No	No	Yes	No
USA – Industry	USI	No	No	Yes	Yes
USA – ORNL	USO	Yes	Yes	Yes	Yes

[a] Unirradiated tests only.

1.4. STRUCTURE OF THE TECDOC

Chapter 2 provides a brief description of both WWER-1000 and PWR reactor pressure vessels, with emphasis on the differences in the materials used for the RPVs. Chapter 3 describes the origin of the CRP WWER-1000 materials and specimens used, plus a summary of the testing and irradiation procedures used by the participants relative to the CRP WWER-1000 materials. Further details on the actual test matrices, test results, and analyses of the results for the CRP WWER-1000 steels are contained in Chapter 4. Similarly, the results of evaluations for the various national steels are described in Chapter 5. Regarding investigations of microstructural effects, Chapter 6 discusses examinations of the WWER-1000 and national steels as well as some detailed discussions of embrittlement mechanisms. Finally, Chapters 7 and 8 present an overall discussion of the results of the CRP and the main conclusions and recommendations for further studies.

2. DESCRIPTION OF REACTOR PRESSURE VESSELS

This chapter provides a description of the Light Water Reactor (LWR) pressure vessels and includes design features, applicable material specifications, and differences amongst the various RPV components especially with respect to the RPV area degraded by irradiation. More detailed information can be found e.g. in Ref. [2.1].

Western-type LWR pressure vessels were designed by Babcock & Wilcox (B&W) Company, Combustion Engineering, Inc., General Electric, Framatome, Mitsubishi Heavy Industries, Ltd, Siemens/KWU, and Westinghouse. The RPVs were fabricated by B&W Company, Chicago Bridge and Iron Company, Combustion Engineering, Inc., Creusot, Klöckner, Rotterdam Dry Dock Company, MAN-GHH, Mitsubishi Heavy Industries, Ltd and Udcomb.

The WWER RPVs were designed by OKB Gidropress, the general designer for all NPPs in the former Soviet Union and the Community for Mutual Economical Assistance (CMEA) countries. Some small modifications were made in the Czech designs by Skoda Co. The WWER plants have been built in two sizes; the WWER-440s which are 440 MWe plants and the WWER-1000s which are 1000 MWe plants. There are two designs for each size; the WWER-440 Type V-230, the WWER-440 Type V-213, the WWER-1000 Type V-302, and the WWER-1000 Type V-320. The Type V-230s were built first and the V-320s were built last. The WWER-440 RPVs are similar as are the WWER-1000 RPVs; the differences in the two designs for the two plant sizes are mainly in the safety systems.

There are only two WWER-1000 Type V-302 pressure vessels, so only WWER-1000 Type V-320 information is presented in this report. The WWER pressure vessels were manufactured at three plants, the Izhora Plant near Saint Petersburg (Russia), the Atommash Plant on the Volga (Russia) and the ŠKODA Nuclear Machinery Plant in the Czech Republic.

2.1. REACTOR PRESSURE VESSEL DESIGN FEATURES

2.1.1. LWR RPVs

A Westinghouse designed RPV is fairly typical of the reactor vessels used in all the so-called Western designed RPVs. However, there are significant differences in size, nozzle designs, penetration designs, and other details among the various suppliers. The RPV is cylindrical with a hemispherical bottom head and a flanged and gasketed upper head. The bottom head is welded to the cylindrical shell while the top head is bolted to the cylindrical shell via the flanges. The cylindrical shell course may or may not utilise longitudinal weld seams in addition to the girth (circumferential) weld seams dependent on the use of rolled plates or ring forgings. The body of the vessel is of low-alloy carbon steel. To minimise corrosion, the inside surfaces in contact with the coolant are cladded with a minimum of about 3 to 10 mm of austenitic stainless steel. Typical design parameters are given in Table 2.1 [2.1] and design end-of-life neutron fluences are summarised in Table 2.2.

An ABB-CE (formally Combustion Engineering) designed RPV is somewhat different than some other western designed RPVs and there are a relatively large number of penetrations which are made from Alloy 600. A Siemens (KWU) designed RPVs significantly differ from other Western design are as follows:

- Set-on inlet and outlet nozzles
- Reinforcement of the flange portion
- No nozzles or guide tubes within the lower part of RPV (no risk of breaks and leaks below the loops)
- One piece upper part section
- Special screwed design for the control rod drive and instrumentation nozzle penetrations made from co-extruded pipe

The French RPVs are designed by Framatome and manufactured by Creusot-Loire.The French RPVs are constructed with ring forging sections and, therefore, there are no longitudinal (vertical) welds. Generally, the core beltline region consists of two parts, although the Sizewell B vessel (UK) has only one ring and some old vessels have three rings in the beltline region

BWR RPVs have usually larger diameters in comparison with PWR with the same reactor output that result in lower neutron fluence on inner RPV wall (Table 2.2) due to a thicker water reflector — water gap between reactor core and RPV.

2.1.2. WWER RPVs

The WWER pressure vessels consist of the vessel itself, vessel head, support ring, thrust ring, closure flange, sealing joint, and surveillance specimens (the latter were not in the WWER/V-230 type of reactors). The WWER RPVs have some significant features that are different from the western designs. A sketch of typical WWER pressure vessels is shown in Figure 2.1 and the main design parameters are listed in Table 2.3.

- The WWER RPVs (as well as all other components) must be transportable by land, i.e. by train and/or by road. This requirement has some very important consequences on vessel design, such as a smaller pressure vessel diameter, which results in a smaller water gap thickness and thus a higher neutron flux on the reactor vessel wall surrounding the core and, therefore, requirements for materials with high resistance against radiation embrittlement.
- Transport by land also results in a smaller vessel mass and, therefore, thinner walls which require higher strength materials.
- The upper part of the vessel consists of two nozzle rings, the upper one for the outlet nozzles and the lower one for the inlet nozzles. An austenitic stainless steel ring is welded to the inside surface of the vessel to separate the coolant entering the vessel through the inlet nozzles from the coolant exiting the vessel through the outlet nozzles. This design results in a rather abrupt change in the axial temperature distribution in the vessel, but uniform temperatures around the circumference.
- The WWER vessels are made only from forgings, i.e. from cylindrical rings and from plates forged into domes. The spherical parts of the vessels, (the bottom and the head) are either stamped from one forged plate, or welded from two plates by electroslag welding, followed by stamping and a full heat treatment. There are no axial welds.

The WWER inlet and outlet nozzles are not welded to the nozzle ring but they are either machined from a thicker forged ring, for the WWER-440 vessels, or forged in the hot stage from a thick forged ring for the WWER-1000 vessels.

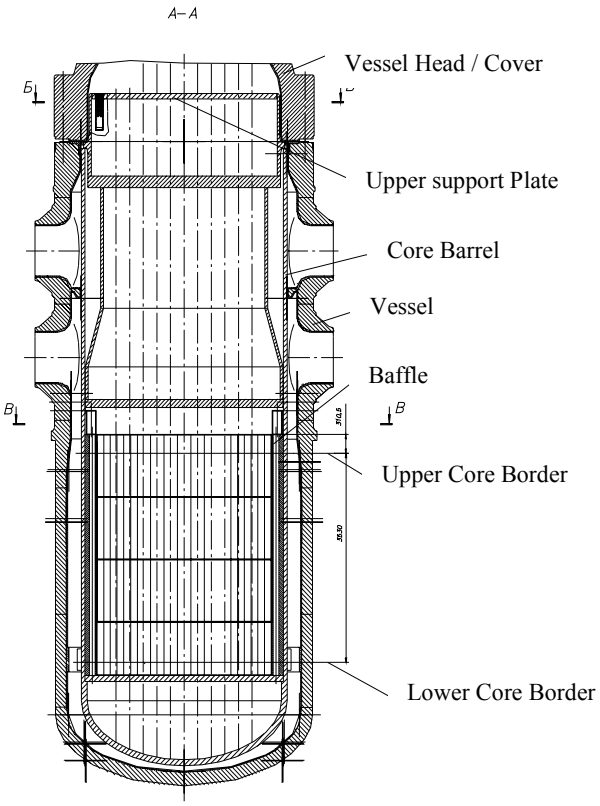

Fig. 2.1. Scheme of WWER-1000 type RPVs.

2.2. VESSEL MATERIALS AND FABRICATION

2.2.1. LWR RPVs

Materials

The western LWR pressure vessels use different materials for the different components (shells, nozzles, flanges, studs, etc.). Moreover, the choices in the materials of construction changed as the LWR products evolved. For example, the Westinghouse designers specified American Society of Mechanical Engineers (ASME) SA 302 Grade B for the shell plates of earlier vessels and ASME SA 533 Grade B Class 1 for later vessels [2.2, 2.3]. Other vessel materials in common use include ASME SA 508 Class 2 plate in the USA, 22NiMoCr37, and 20MnMoNi55 in Germany, and 16MnD5 in France. In addition to using plate products, all the NSSS vendors also use forgings in the construction of the shell courses. Table 2.4 lists the main ferritic materials used for LWR vessel construction over the years and summarises their chemical composition [2.4]. Table 2.5 lists the various materials used for beltline region of LWR RPVs.

SA-302, Grade B is a manganese-molybdenum plate steel used for a number of vessels made through the mid-1960s. Its German designation is 20MnMo55. As commercial nuclear power evolved, the sizes of the vessels increased. For the greater wall thickness required, a material with greater harden ability was necessary. The addition of nickel to SA-302, Grade B in amounts between 0.4 and 0.7 weight percent provided the necessary increased harden ability to achieve the desired yield strength and high fracture toughness across the entire wall thickness. This steel was initially known as SA-302, Grade B Ni Modified.

Forging steels have also evolved since the mid-1950s. The SA-182 F1 Modified material is a manganese-molybdenum-nickel steel used mostly for flanges and nozzles in the 1950s and 1960s. Another forging material used then was a carbon-manganese-molybdenum steel, SA-336 F1. Large forgings of these materials had to undergo a cumbersome, expensive heat treatment to reduce hydrogen blistering. Eventually these steels were replaced with a newer, that did nor require this heat treatment and was described first described as ASTM A366 Code Case 1236 but is now known as SA-508 Class 2 [2.5]. This steel has been widely used in ring forgings, flanges, and nozzles.

It was introduced into Germany with the designation 22NiMoCr36 or 22NiMoCr37. With slight modifications, this steel became the most important material for German reactors for a long time. Additionally, SA-508 Class 3 (20MnMoNi55 in Germany and 16 MnD5 and 18MnD5 in France) is used in the fabrication of Western RPVs.

Although many materials are acceptable for reactor vessels according to Section III of the ASME Code, the special considerations pertaining to fracture toughness and radiation effects effectively limit the basic materials currently acceptable in the U.S. for most parts of vessels to SA-533 Grade B Class 1, SA-508 Class 2, and SA-508 Class 3 [2.6].

The part of the vessel of primary concern with regard to age related degradation is the core beltline-the region of shell material directly surrounding the effective height of the fuel element assemblies plus an additional volume of shell material, both below and above the active core, with an end-of-life fluence of more than 10^{21} m^{-2} ($E > 1$ MeV). It is typically located in the intermediate and lower shells. The low alloy steels making up the beltline are subject to irradiation embrittlement that can lead to loss of fracture toughness.

When early vessels were designed and constructed, only limited data existed about changes in material properties caused by radiation damage. Now it is known that the susceptibility of RPV steels is strongly affected by the presence of copper, nickel, and phosphorus. Because operating vessels fabricated before 1972 contain relatively high levels of copper and phosphorous, irradiation damage becomes a major consideration for their continued operation.

The French have recently introduced the use of hollow ingots to make the beltline ring sections. The beltline material used in France is 16 MnD5. The chemical requirements for this material are listed in Table 2.4 along with the other Western materials. As a general rule, material with a tensile strength at room temperature above 700 MPa cannot be used for pressure boundaries. The other western RPVs are designed with a minimum tensile strength of 350 MPa (50 ksi) – Table 2.8.

Fabrication practices

Fabrication of RPVs has also been an evolving technology, and later vessels were fabricated using knowledge gained from the surveillance programmes and more modern methods such as the use of large ring forgings to reduce the number of welds in the beltline [2.5, 2.7].

Large vessels are fabricated by two methods. In the first method, rolled and welded plates are used to form separate steel courses. Such a vessel has both longitudinal and circumferential weld seams. In some older vessels (before 1972), the longitudinal welds are of particular concern with regard to vessel integrity because they contain high levels of copper

and phosphorous. In the second method, large ring forgings are used. This method improves component reliability because of the lack of longitudinal welds. Weld seams are located to avoid intersection with nozzle penetration weldments.

Weldments within the beltline region were minimised once research showed that weld metal could be more sensitive to neutron radiation than base material and can have higher flaw density than base metals. In general, parts of the longitudinal shell course welds are within the beltline region when the RPV is fabricated using plate material. At least one circumferential weld is near, or marginally within, the beltline region when the RPVs are fabricated from either plates or ring forgings. Recently, Nuclear Steam Supply System (NSSS) vendors are designing the RPV such that the beltline region does not contain any weldments. This is accomplished by utilising very large ring forgings to fabricate the shell course.

The interior surfaces of the steel vessel, closure head, and flange area are typically clad with stainless steel, usually Type 308 or 309. Cladding is used to prevent general corrosion by borated coolant and to minimise the build-up of corrosion products in the reactor coolant system. The cladding is variously applied in one or two layers by multiple-wire, single-wire or strip-cladding techniques, all or resistance welding processes. Some vessels have areas of Alloy 82 or 182 weld cladding where Alloy 600 components are welded to the vessel.

Welding

The welding processes used are mostly submerged-arc and shielded-metal-arc. Before the early 1970s, copper-coated weld wire was used to improve the electrical contact in the welding process and to reduce corrosion during storage of the weld wire, hence the potential generation of hydrogen. When it was discovered that copper and phosphorus increased the weld's sensitivity to radiation embrittlement, RPV fabricators imposed strict limits on the percentage of copper and phosphorus in the welds as well as in plates [2.5, 2.8, 2.9]. The use of copper coated weld wire was subsequently eliminated due to the strict limits on the percentage of copper in the weld. The weld wire or stick electrodes were kept in storage in plastic bags and/or low temperature furnaces to eliminate the formation of moisture on the weld wire and electrodes.

For the circumferential welds, many weld passes, and consequently a large volume of weld wire are needed. This becomes important when determining the properties of each individual weld in the beltline for sensitivity to neutron irradiation. For example, the chemistry of the weld (copper and nickel content) may vary through the thickness and around the circumference because of variations in the weld wire used in fabrication. Each weld in the vessel can be traced by the unique weld wire and flux lot combination used [2.7].

The sensitivity of welds to radiation can be inferred from the chemical composition. The degree of embrittlement [shift in transition temperature or decrease in upper shelf energy (USE)] is determined as a function of the chemical composition and the level of neutron exposure. Copper, nickel, and phosphorus content in the weld are the most important elements from the standpoint of radiation damage. The embrittlement of high copper and high nickel welds plays a key role in the assessment of the significance of pressurised thermal shock (PTS) [2.7].

2.2.2. WWER RPVs

The WWER pressure vessel materials are listed in Table 2.5 and the major design parameters in Table 2.3. The chemical compositions of the various WWER materials are listed in Table 2.6. The allowable impurities in the beltline region are listed in Table 2.7, and the guaranteed mechanical properties are listed in Table 2.8. As indicated by the information in these tables, the WWER pressure vessel materials are basically different than the Western RPV materials. The Type 15Kh2MFA(A) material used for the WWER-440 pressure vessels contains 0.25 to 0.35 mass percent vanadium and very little nickel (maximum of 0.40 mass percent).

The Type 15Kh2NMFA(A) material used for the WWER-1000 pressure vessels contains 1.0 to 1.5 mass percent nickel (in welds up to 1.9 mass percent) and almost no vanadium. Material with vanadium alloying was first used in the former Soviet Union naval RPVs because the vanadium carbides make the material relatively resistant to thermal ageing, fine grained (tempered bainite), and strong. However, the Type 15Kh2MFA(A) material is more difficult to weld than nickel steels and requires very high preheating to avoid hot cracking. This became more of a problem for the large WWER-1000 pressure vessels and a material with nickel rather than vanadium alloying was chosen. The influence of vanadium on the susceptibility of those materials to radiation embrittlement was shown to be negligible.

Not all the WWER pressure vessels were covered by austenitic stainless steel cladding on their whole inner surface: only approximately half of the WWER-440/V-230 pressure vessels were clad. However, all of the WWER-440/V-213 and WWER-1000 pressure vessels were covered on the whole inner surface. The cladding was made by automatic strip welding under flux with two layers — the first layer is made of a Type 25 chromium/13 nickel nonstabilized austenitic material (Sv 07Kh25N13), and the second layer is at least three passes made of Type 18 chromium/10 nickel stabilized austenitic stainless steel (Sv 08Kh18N10G2B) to achieve a required total thickness of cladding equal to 8^{+2}_{-1} mm. Therefore, all the austenitic steels which are in contact with water coolant are stabilised.

The stabilize daustenitic stainless steels for cladding contain an alloying element (niobium) which forms stable gain boundary carbides. This prevents chromium depletion along the grain boundaries and makes the material immune to stress corrosion cracking. Unstabilized material was used for the first layer because the thermal expansion coefficient of that material is closer to the thermal expansion coefficient of the low-alloy pressure vessel material.

The WWER vessel head contains penetrations with nozzles. The nozzles are welded to the vessel head from inside (buttering) and are protected by stainless steel sleeving (0Kh18N10T). List of abbreviations used for nomenclature of WWER materials based on their chemical composition is given in Table 2.9.

Table 2.1. Major characteristics of typical LWR RPVs

Major Parameters	French 4-loop N4 Type Plants	German Konvoi Design Values	Westinghouse 4-Loop Plant
Thermal power (MWth)	4,270	3,765	3,411
Electric output (MWe)	1,475	> 1,300	1,125
Number of loops	4	4	4
Active core length (mm)	4,270	3,900	3,660
Core diameter (mm)	4,490	3,910	3,370
Water gap width* (mm)	424	545	512
Linear heating rate (W/cm)	179	166.7	183
Vessel outlet temperature (°C)	329.5	326.1	325.5
Outlet/inlet temperature difference (°C)	37.5	34.8	33.0
Specified initial RT_{NDT}		-12°C	
** ΔT_{41J} at EOL (based on design values)		23°C	

* Distance from the outer fuel element and the RPV inner surface.

** ΔT_{41J}: shift in Charpy 41 J transition temperature, °C

Table 2.2. Design end-of-life fluence for WWERs, PWRs and the BWR

REACTOR TYPE	FLUX, $m^{-2}.s^{-1}$ (E>1MeV)	LIFETIME* FLUENCE, m^{-2} (E>1MeV)
WWER-440 core weld	1.2×10^{15}	1.1×10^{24}
WWER-440 maximum	1.5×10^{15}	1.6×10^{24}
WWER-1000	$3\text{-}4 \times 10^{14}$	3.7×10^{23}
PWR (W)	4×10^{14}	4×10^{23}
PWR (B&W)	1.2×10^{14}	1.2×10^{23}
BWR	4×10^{13}	4×10^{22}

* Lifetime fluence for WWERs are calculated for 40 calendar years, PWRs are calculated for 32 Effective Full Power Year. But also note that this does not include the effect of service or operational life extension.

Table 2.3. WWER pressure vessel design parameters and materials

Reactor	WWER-440		WWER-1000
	V-230	V-213	V-320
mass [t]	215		320
Length [mm]	11,800		11,000
outer diameter [mm]			
- in cylindrical part	3,840		4,535
- in nozzle ring	3,980		4,660
wall thickness (without cladding) [mm]			
- in cylindrical part	140		193
- in nozzle ring	190		285
number of loops	6		4
working pressure [MPa]	12.26		17.65
operating wall temperature [°C]	265		288
Design wall temperature [°C]	325		350
vessel lifetime [y]	30	40	40

[a] The fast fluence at energies greater than 0.5 MeV is about 1.67 times the fast fluence at energies greater than 1.0 MeV

Table 2.4. Chemical requirements (heat analysis) – main ferritic materials for reactor components in LWR RPVs

Designation	C	Si	Mn	P_{max}	S_{max}	Elements (mass %)				Cu_{max}	Al	Sn	N2	As
						Cr	Mo	Ni	V_{max}					
ASTM A 302B	max 0.25	0.15 0.30	1.15 1.50	max 0.035	max 0.040		0.45 0.60							
ASTM A 336, Code Case 1236	0.19 0.25	0.15 0.35	1.10 1.30	max 0.035	max 0.035	max 0.35	0.50 0.60	0.40 0.50						
ASME A 508 Cl 2 (1971)	max 0.27	0.15 0.35	0.50 0.90	max 0.025	max 0.025	0.25 0.45	0.55 0.70	0.50 0.90	max 0.05					
ASME A 533 GR B (1971)	max 0.25	0.15 0.30	1.15 1.50	max 0.035	max 0.040		0.45 0.60	0.40 0.70						
ASME A 508 Cl 2 (1989)[1]	max 0.27	0.15 0.40	0.50 1.00	max 0..015	max 0.015	0.25 0.45	0.55 0.70	0.50 1.00	max 0.05	max 0.15				
ASME A 508 Cl 3 (1989)[1]	max 0.25	0.15 0.40	1.20 1.50	max 0.015	max 0.015	max 0.25	0.45 0.60	0.40 1.00	max 0.05					
ASME A 533GRr B (1989)	max 0.25	0.15 0.40	1.15 1.50	max 0.035	max 0.040		0.45 0.60	0.40 0.70						
16 MnD5 RCC-M 2111[2]	max 0.22	0.10 0.30	1.15 1.60	max 0.02	max 0.012	max 0.25	0.43 0.57	0.50 0.80	max 0.01	max 0.20	max 0.040			
18 MnD5 RCC-M 2112 (1988)	max 0.20	0.10 0.30	1.15 1.55	max 0.015	max 0.012	max 0.25	0.45 0.55	0.50 0.80	max 0.01	max 0.20	max 0.040			
20 Mn Mo Ni 5 5 (1983, 1990)[3] [4]	0.17 0.23	0.15 0.30	1.20 1.50	max 0.012	max 0.008	max 0.20	0.40 0.55	0.50 0.80	max 0.02	max 0.12[5]	0.010 0.040	max 0.011	max 0.013	max 0.036
22 Ni Mo Cr 3 7 (1991)[6]	0.17 0.23	0.15 0.35	0.50 1.00	max 0.012	max 0.008	0.25 0.50	max 0.60	0.60 1.20[7]	max 0.02	max 0.12[5]	0.010 0.050	max 0.011	max 0.013	max 0.036

[1] Supplementary Requirement S 9.1(2) and S 9.2 for A 508 cl 2 and 508 cl 3.
[2] Forgings for reactor shells outside core region. Restrictions for Core Region (RCC-M 2111): S≤0.008, P≤0.008, Cu≤0.08.
[3] VdTÜV Material Specification 401, Issue 1983.
[4] KTA 3201.1 Appendix A, Issue 6/90.
[5] Cu-Content for RPV (Core Region) shall be ≤0.10%.
[6] According *Siemens/KWU* under consideration of SR 10 (MPa Stuttgart).
[7] For flanges and tube sheets the Ni-content shall be ≤1.40%.

Table 2.5. Materials used for beltline region of LWR RPVs

COUNTRY	**SHELLS**	**AUSTENITIC CLADDING**
USA	SA302 GR B SA533 GR B, Class 1 SA 508 Class 2 SA 508 Class 3	TYPE 308L, 309L TYPE 304
France	16MnD5	
GERMANY	20MnMoNi55 22NiMoCr3 7	
WWER-440	15Kh2MFA(A)	Sv 07Kh25N13 – 1st layer Sv 08Kh19N10G2B – 2nd layer
WWER-1000	15Kh2NMFA(A)	

Table 2.6. Chemical composition of WWER forging and weld materials (mass%)

MATERIAL	C	Mn	Si	P	S	Cr	Ni	Mo	V
2.2.2.1. WWER-440 15Kh2MFA		0.30 0.60	0.17 0.37	max 0.025	max 0.025	2.50 3.00	max 0.40	0.60 0.80	0.25 0.35
Submerged arc weld Sv-10KhMFT + AN-42	0.04 0.12	0.60 1.30	0.20 0.60	max. 0.042	max 0.035	1.20 1.80	max 0.30	0.35 0.70	0.10 0.35
Submerged arc weld Sv-10KhMFT + AN-42M	0.04 0.12	0.60 1.30	0.20 0.60	max 0.012	max 0.015	1.20 1.80	max 0.30	0.35 0.70	0.10 0.35
Electroslag weld Sv-13Kh2MFT + OF-6	0.11 0.16	0.40 0.70	0.17 0.35	max 0.030	max 0.030	1.40 2.50	-	0.40 0.80	0.17 0.37
2.2.2.2. WWER-1000 15Kh2NMFA	0.13 0.18	0.30 0.60	0.17 0.37	max 0.020	max 0.020	1.80 2.30	1.00 1.50	0.50 0.70	max 0.10
Submerged arc weld Sv-12Kh2N2MA + FC-16	0.05 0.12	0.50 1.00	0.15 0.45	max 0.025	max 0.020	1.40 2.10	1.20 1.90[x]	0.45 0.75	
Submerged arc weld Sv-12Kh2N2MA+ FC-16	0.05 0.12	0.50 1.00	0.15 0.45	max 0.012	max 0.015	1.40 2.10	1.20 1.9[x]	0.45 0.75	-

Table 2.7. Allowable impurity content in the WWER and LWR beltline materials (max. mass %)

MATERIAL	P	S	Cu	As	Sb	Sn	P+Sb+Sn	Co
15Kh2MFAA	0.012	0.015	0.08	0.010	0.005	0.005	0.015	0.020
15Kh2NMFAA	0.010	0.012	0.08	0.010	0.005	0.005	0.015	0.020
A 533-B, Class 1	0.012	0.015	0.10	-	-	-	-	-

Table 2.8. Guaranteed mechanical properties of LWR/WWER RPV materials*

MATERIAL	20 ^{O}C				350 ^{O}C				T_{k0} (1) RT_{NDT} (2)
	$R_{p0.2}$	R_m	A_5	Z	$R_{p0.2}$	R_m	A_5	Z	
	[Mpa]	[MPa]	[%]	[%]	[MPa]	[MPa]	[%]	[%]	[^{O}C]
15Kh2MFA - base metal	431	519	14	50	392	490	14	50	0(1)
- A/S weld metal	392	539	14	50	373	490	12	45	20(1)
15Kh2NMFA - base metal	490	608	15	55	441	539	14	50	-10(1)
15Kh2NMFAA - base metal	490	608	15	55	441	539	14	50	-25(1)
- A/S weld metal	422	539	15	55	392	510	14	50	0(1)
A 533-B, Cl.1	345	551	18	-	285	-	-	-	-12(2)
A 508, Cl.3	345	551	18	38	285	-	-	-	-12(2)

*$R_{p0.2}$ is the 0.2 percent offset yield strength, R_m is the ultimate tensile strength, Z is the percent reduction in area at failure, and
(1) T_{k0} is the initial ductile-brittle transition temperature for WWER materials
(2) RTNDT is the initial ductile-brittle transition temperature for LWR materials.

Table 2.9. List of abbreviations used in WWER materials

Chemical elements:	A	high quality
	AA	very high quality/purity
	B	niobium
	F	vanadium
	G	manganese
	Kh	chromium
	M	molybdenum
	N	nickel
	Sv	welding wire
	T	titanium
Beginning of the designation:	0	less than 0.1 mass %
	08	mean value 0.08 %
	15	mean value 0.15 %
Centre of the designation:	Kh2	mean value 2 %
	M	lower than 1 %

2.3. DESIGN BASIS: CODES, REGULATIONS AND GUIDES FOR REACTOR PRESSURE VESSELS

2.3.1. LWR RPVs

The load restrictions on as-fabricated RPVs in various national standards and codes are generally based on Section III of the ASME Boiler and Pressure Vessel Code [2.11]. The objective of designing and performing a stress analysis under the rules of Section III to the ASME Boiler and Pressure Vessel Code is to afford protection of life and property against ductile and brittle RPV failure. Some important differences exist in the RPV design requirements of certain other countries (e.g. Germany, France).

ASME section iii design basis

The reactor vessel has been designated as Safety Class 1 which requires more detailed analyses than Class 2 or 3 components. The rules for Class 1 vessel design are contained in Article NB-3000, which is divided into three sub-articles:

a. NB-3100, General Design Rules
b. NB-3200, Design by Analysis
c. NB-3300, Vessel Design

Sub-article NB-3100 deals with Loading Conditions specified by the Owner (or his agent) in the form of an Equipment Specification. The specification identifies the Design Conditions and Operating Conditions (Normal Conditions, Upset Conditions, Emergency Conditions, Faulted Conditions, and Testing Conditions).

Sub-article NB-3200 deals with the stresses and stress limits which must be considered for the analysis of the component. The methods of analysis and stress limits depend upon the category of loading conditions, i.e. the requirement for Normal Conditions are considerably more stringent than those for Faulted Conditions.

Sub-article NB-3300 gives special requirements that have to be met by Class 1 vessels. This article gives tentative thickness requirements for shells, reinforcement requirements for nozzles, and recommendations for welding nozzles, for example.

Part 50 of the U.S. Code of Federal Regulations, Title 10 (10 CFR 50) regulates the construction of NPPs [2.12]. Section 10 CFR 50.55(a) defines the reactor vessel to be part of the reactor coolant boundary and requires that the vessel meet the requirements contained in the ASME Boiler and Pressure Vessel Code Sections III for Class 1 vessels.

The **German** reactor vessel designs follow the German KTA standards for light water reactors, published by the NUSS Commission. The KTA requirements are very similar to those in the ASME code regarding the definition of stress intensities and allowable stresses. However, considerable differences exist in the design requirements for Upper Shelf Energy (USE) and mid-thickness tensile and Charpy values, as well as for in-service inspections. Also, the new German KTA has a limit on the allowable fluence whereas the ASME Code and the codes in a number of other countries do not.

The oldest **French** 3-loop plants were designed under ASME Section III, Appendix G [2.13]. The newer 4-loop plants are being designed under RCC-M B 3200, Appendix ZG [2.14]. The RCC-M B 3200 rules are similar to the rules in ASME Section III (however, the fabrication, welding, examination and QA rules are different) [2.15, 2.16].

2.3.2. WWER RPVs

The RPVs and primary system piping for all WWERs are safety related components and must be evaluated according to the former Soviet Codes and Rules [2.17 – 2.20]. With respect to the WWER RPVs, special analysis requirements are also provided for radiation embrittlement. The Codes [2.19, 2.20] are divided into 5 parts:

(1) *General Statements* deals with the area of Code application and basic principles used in the Code.
(2) *Definitions* gives full description of the most important operational parameters as well as parameters of calculations.
(3) *Allowable stresses, strength and stability conditions*
(4) *Calculation of basic dimensions* deals with the procedure for choosing the component wall thickness, provides strength decrease coefficients and hole reinforcement values. Further, formulae for analysis of flange and bolting joints are also given.
(5) *Validating calculations* are the most important part of the Code. These detailed calculations contain rules for the classification of stresses as well as steps for stress determination.

Further, detailed calculations for different possible failure mechanisms are required and their procedures and criteria are given:

- Calculation of static strength,
- Calculation of stability,
- Calculation of cyclic strength (fatigue),
- Calculation of resistance against brittle fracture,
- Calculation of seismic effects,
- Calculation of vibration strength (ultra-high frequency fatigue).

A mandatory part of this Code contained in appendices is also a list of the materials (and their guaranteed properties) to be used for manufacturing the components of the NSSS, including the RPVs. These appendices also contain methods for the determination of the mechanical properties of these materials and some formulas for designing certain structural features (e.g. nozzles, closures etc.) of the vessel, as well as typical equipment units strength calculations.

REFERENCES

[2.1] INTERNATIONAL ATOMIC ENERGY AGENCY, Assessment and management of ageing of major nuclear power plant components important to safety: PWR pressure vessels, IAEA-TECDOC-1120, Vienna, (1999).

[2.2] AMERICAN SOCIETY FOR TESTING AND MATERIALS, Annual Book of ASTM Standards, Section 1 – "Iron and Steel Products", Volume 01.04 – "Steel, Structural, Reinforcing, Pressure Vessel, Raillway" (1989).

[2.3] AMERICAN SOCIETY FOR MECHANICAL ENGINEERS, ASME Boiler and Pressure Vessel Code, Section II, "Materials Specifications", Part A, "Ferrous Materials", New York (1995).

[2.4] TENCKHOFF, E., ERVE, M., "Materials for Nuclear Power Plants in Western Countries", in Sonderdruck aus Atomwirtschaft, Jahrgang XXXVII, No. 4 (1992)

[2.5] GRIESBACH, T.J., SERVER, W.L., Reactor Pressure Vessel Embrittlement Management Handbook, Rep.TR-101975-T2, Electric Power Research Institute, Palo Alto, CA, USA (1993).

[2.6] U.S. NUCLEAR REGULATORY COMMISSION, Standard Review Plan for the Review of Safety Analysis Reports for Nuclear Power Plans, LWR Edition, Section 5.3.3., "Reactor Vessel Intengrity", Rep. NUREG-0800, USNRC, Washington, DC, USA (1981).

[2.7] U.S. NUCLEAR REGULATORY COMMISSION, Reactor Pressure Vessel Status Report, Rep. NUREG-1511, USNRC, Washington, DC, USA (1994).

[2.8] WHITMAN, D.G., ET AL., Technology of Steel Pressure Vessel for Water Cooled Nuclear Reactors, ORNL-NSIC-21, Oak Ridge National Laboratory, Oak Ridge, TN, USA (1967).

[2.9] GRIESBACH, T.J., SERVER, W.L., Reactor Pressure Vessel Embrittlement Management Handbook, Rep.TR-101975-T2, Electric Power Research Institute, Palo Alto, CA, USA (1993).

[2.10] ELECTRIC POWER RESEARCH INSTITUTE, White Paper on Reactor Vessel Integrity Requirements for Level A and B conditions, Rep.TR-100251, EPRI, Palo Alto, CA, USA (1993).

[2.11] AMERICAN SOCIETY OF MECHANICAL ENGINEERS, ASME Boiler and Pressure Vessel Code, Section III, "Nuclear Power Plant Components", ASME, New York, USA (1995).

[2.12] U.S. Code of Federal Regulation, Part 10 – Energy Office of the Federal Register, National Archives and Records Administration, Washington, DC, USA (1995).

[2.13] AMERICAN SOCIETY OF MECHANICAL ENGINEERS, ASME Boiler and Pressure Vessel Code, Section III, "Nuclear Power Plant Components", Appendix G, "Protection Against Non-ductile Failure", New York, USA (1995).

[2.14] ASSOCIATION FRANÇAISE POUR LES REGLES DE CONCEPTION ET DE CONSTRUCTION DES MATERIELS DE CHAUDIERES ELECTRO-NUCLEAIRES, Règles de conception et de cosstruction de matériels mécaniques des îlots nucléaires PWR. RCC-M, AFCEN, Paris, France (1995).

[2.15] BAYLAC, G., GRANDEMANGE, J.M., “The French Code RCC-M: Design and construction rules for the mechanical components of PWR nuclear islands”, Nuclear Engineering and Design 129 pp 239–254 (1991).
[2.16] FAIDY, G., “The French Design Code: RCC-M status and ongoing developments, pressure vessels and piping codes and standards”, Proc. ASME Pressure Vessel and Piping Conf., Montreal, USA (1996).
[2.17] Rules for Design and Safe Operation of Components in NPPs, Test and Research Reactors and Stations, Metallurgia, Moscow, Russia (1973).
[2.18] Rules for Design and Safe Operation of Components and Pipin g of NPP, PNAE G-7-008-89, Energoatomizdat, Moscow, Russia (1990).
[2.19] Code for Strength Calculations of Components of Reactors, Steam Generators and Piping in NPPs, Test and Research Reactors and Stations, Metallurgia, Moscow, Russia (1973).
[2.20] Code for Strength Calculations of Components and Piping in Nuclear Power Plants, Energoatomizdat, Moscow, Russia (1989).

3. DESCRIPTION OF CRP MATERIALS AND PROCEDURES

3.1. DESCRIPTION OF CRP MATERIALS

To conduct the experimental investigations regarding nickel influence on radiation embrittlement of WWER-1000 RPV metals, RRC "Kurchatov Institute" (RRC KI) offered two materials with different nickel content, one base metal and one weld metal. The material chemical compositions are presented in Table 3.1.

Table 3.1. Chemical composition of WWER-1000 materials

Material	Chemical composition, mass %									
	C	Si	Mn	Cr	Ni	Cu	S	P	V	Mo
Base metal 15Kh2NMFAA	0.17	0.30	0.46	2.2	1.26	0.05	0.010	0.008	0.10	0.50
Weld metal 12Kh2N2MAA	0.11	0.14	0.73	1.9	1.7	0.06	0.008	0.006	0.01	0.55

To investigate nickel influence on the radiation embrittlement of these WWER-1000 type steels, it was proposed that standard Charpy V-notch (CVN) impact specimens be prepared and distributed by RRC KI to participants of the project. The guidance was given to participants for the conduct of irradiation experiments incorporated irradiation to a neutron fluence not less than the neutron fluence on the inside wall of the WWER-1000 RPV at the end of its design lifetime [~$5x10^{19}$ n/cm^2 (E>0.5 MeV)] and at the temperature which corresponds to the beltline region of the WWER-1000 RPV (290°C). It was also proposed to make tensile specimens from the halves of broken Charpy specimens. As presented later, not all participants' irradiation experiments achieved the desired fluence nor were tensile specimens machined from broken Charpy specimens.

The scheme for cutting templates from the shell is shown in Fig. 3.1. From the templates, then, Figures 3.2 and 3.3 show the schemes for cutting layers which were used for machining Charpy specimens (including V-notches). A total of 48 CVN specimens, 12 for testing of each material in both unirradiated and irradiated conditions were provided to each participant that performed Charpy testing. Tensile testing was performed by RRC-KI and the results provided to all participants.

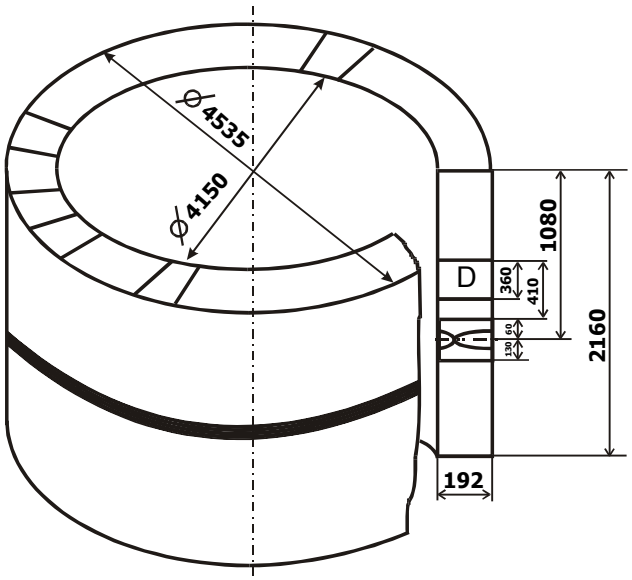

Fig. 3.1. Scheme for cutting templates from the shell of a WWER-1000 RPV.

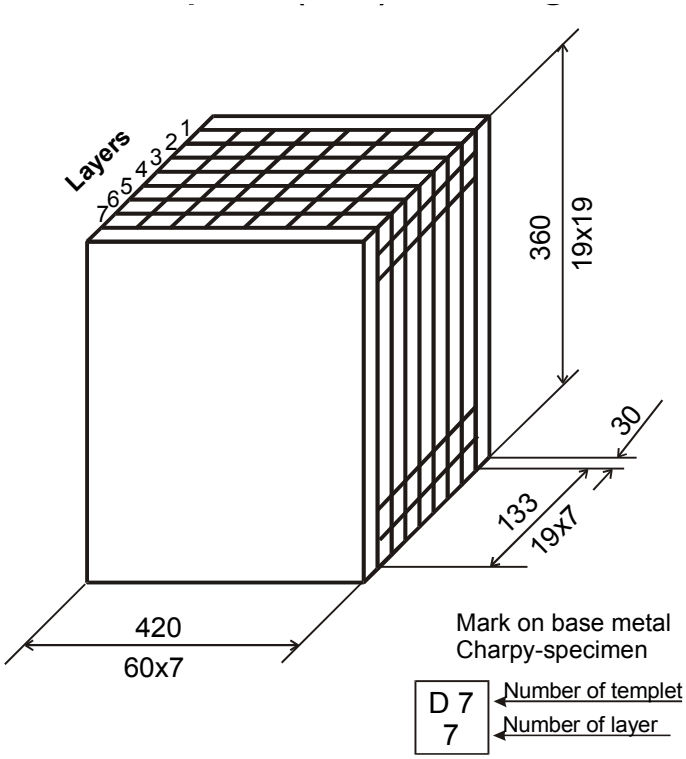

Fig. 3.2. Scheme for cutting layers of base metal from templates.

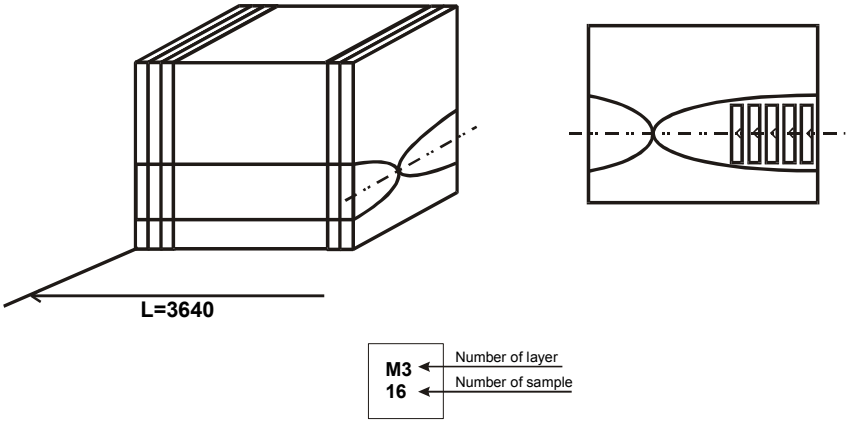

Fig.3.3 Scheme for cutting layers of weld metal from templates.

Table 3.2. Identification of machined specimens and orientations

Material WWER-1000	Identification	Number and mark of layer	Orientation of Charpy specimens[a]	Orientation of tensile specimens
Base metal	106139	7 D7-7	L-T	L
Weld metal	177271	3, 4 M3, M4	T-L	T

[a] For base metal, orientation designation follows ASTM E-399 [3.1]. For weld metal, T means transverse to the welding direction and L means the welding direction.

3.2. IRRADIATION CONDITIONS AND TEST PROCEDURES

As discussed in section 3.1, CVN specimens were prepared and supplied by RRC-KI to each participant. In the case of base metal specimens irradiated and tested by NRI, NRI fabricated inserts from previously tested unirradiated Charpy halves. Following irradiation, the inserts were then used to make reconstituted CVN specimens and tested. Table 3.3 provides a summary of CVN test procedures and irradiation conditions for the WWER-1000 materials that constitute the mandatory part of this CRP.

All participants performed CVN impact tests according to ISO/EN10045, except for the USA-ORNL which utilized the ASTM E23 [3.2] test standard and the ASTM tup. The ISO tup has a 2-mm radius while the ASTM tup has an 8-mm radius. References [3.3] and [3.4] provide information regarding the effects of these tup differences on a number of different steels. Essentially, for typical RPV steels, there are no significant differences in the impact energy up to about 175 J, but Reference [3.4] observed a consistent difference in lateral expansion results with the 2 mm tup resulting in somewhat greater values up to about 8%.

For the purposes of this study, as shown in Table 3.3, some of the irradiations were conducted in power reactors and some in research reactors, with fast neutron fluxes (>0.5 MeV) varying from 5.1×10^{11} to 5.0×10^{13} n/cm^2·s (>0.5 MeV). Moreover, the total exposures varied from 2.4×10^{19} to 14.9×10^{19} n/cm^2 (>0.5 MeV), providing the opportunity to evaluate the embrittlement as a function of fluence. Additional consideration must be given to irradiation temperature, as that parameter has been shown to significantly affect the irradiation-induced embrittlement of RPV steels [3.5].

Table 3.3. Summary of test procedures and irradiation conditions for CRP WWER-1000 steels

Country/Laboratory	CVN Test Procedure/Tup[b]	Irradiation Conditions				
		Reactor		Flux, n/cm^2·s (>0.5 MeV)	Fluence n/cm^2 (>0.5 MeV)	Temp °C
		Type	Name			
Bulgaria-Bulgarian Academy of Sciences Institute of Metal Science	ISO/ISO	WWER-1000 Surveillance Channels	Kozloduy NPP-Unit 5	~3x10^{12}	Weld Metal: 8.8x10^{19}	292±5
Czech Republic – NRI	ISO[a]/ISO	Research	LVR-15	~1.5x10^{13}	All: 14.7x10^{19}	290±10
Hungary-KFKI-Atomic Energy-Research Institute	ISO/ISO	Research	VVR-S	3.3x10^{13}	All: 5.5x10^{19}	290±10
Russia-Kurchatov Institute	ISO/ISO	WWER-1000 Surveillance Channels	Novovoronezh NPP-Unit 5	~2-5x10^{12}	Base Metal: 9.5x10^{19} 14.9x10^{19} Weld Metal: 5.2x10^{19} 6.5x10^{19} 11.5x10^{19}	292±5
Russia – Prometey	ISO/ISO	Research	WWR-M	Base Metal: 2.2x10^{13} 1.1x10^{13} 3.4x10^{13} Weld Metal: 2.3x10^{13} 5.0x10^{13}	Base Metal: 2.8x10^{19} 2.9x10^{19} 5.6x10^{19} Weld Metal: 2.8x10^{19} 5.0x10^{19}	290±10 280±10 285±10 290±10 285±10
USA – ORNL	ASTM/ASTM	Research	Ford Reactor	5.1x10^{11}	All: 2.37x10^{19}	288±2

[a] Reconstituted specimens were tested in the irradiated conditions.
[b] Tup is an end of the pendulum which strikes into the specimen.

REFERENCES

[3.1] AMERICAN SOCIETY FOR TESTING AND MATERIALS, Standard Test Method for Plane-Strain Fracture Toughness of Metallic Materials. ASTM E 399, Annual Book of Standards, Vol. 03-01, ASTM International, West Conshohocken, PA, 2004.

[3.2] AMERICAN SOCIETY FOR TESTING AND MATERIALS, Standard Method for Notched Bar Impact Testing of Metallic Materials. ASTM Standard E-23, Annual Book of Standards, Vol. 03-01, ASTM International, West Conshohocken, PA, 2004.

[3.3] NANSTAD, R. K. AND SOKOLOV, M. A., "Charpy Impact Test Results on five Materials and NIST Verification Specimens Using Instrumented 2-mm and 8-mm Strikers," Pendulum Impact Machines: Procedures and Specimens for Verification, ASTM STP 1248, Thomas A. Siewert and A. Karl Schmieder, Eds., American Society for Testing and Materials, Philadelphia, 1995.

[3.4] NANIWA, T., ET. AL., "Effects of the Striking Edge Radius on the Charpy Impact Test," Charpy Impact Test: Factors and Variables, ASTM STP 1072, John M. Holt, Ed., American Society for Testing and Materials, Philadelphia, 1990.

[3.5] INTERNATIONAL ATOMIC ENERGY AGENCY, Neutron Irradiation Embrittlement of LWR Reactor Pressure Vessels; IAEA-TRS-XXX under preparation.

4. RESULTS AND ANALYSIS OF CRP WWER-1000 STEELS TESTS

4.1. INTRODUCTION

As stated in Chapter 3, most of the participants tested the CRP WWER-1000 base and weld metals in both the unirradiated and irradiated conditions. A target fluence range was provided as a guideline, but each participant irradiated the specimens as allowed within their institutional programs and the results provide a reasonably wide range of fluence with which to compare results with normative standards. In this chapter, the results shown for 41J transition temperatures, upper-shelf energies, and neutron fluences are those provided by the participants, while the irradiation-induced 41J temperature shifts and various adjustments are those performed during the preparation of this report.

4.2. TRANSITION TEMPERATURE TEST RESULTS

Summaries of the results of this CRP are given in Table 4.1 for base metal and in Table 4.2 for the weld metal. In the tables, the unirradiated 41J transition temperature is designated as $T_{41J\text{-}UN}$, while that for the irradiated condition is designated as $T_{41J\text{-}IRR}$. Also, the irradiation-induced 41J temperature shift as calculated from the T_{41J} measurements of the participants is designated ΔT_{41J}.

Table 4.1. Summary of test results for CRP WWER-1000 base metal

Participants	Country	Fluence 10^{19} n/cm^2	$T_{41J\text{-}UN}$	$T_{41J\text{-}IRR}$	ΔT_{41J}	$T_{41J\text{-}ADJ}$	$\Delta T_{41J\text{-}ADJ}$
		E>0.5MeV	ºC	ºC	ºC	ºC	ºC
Kuchatov Institute	Russia	9,5	**-81**	-29	52	**-83**	54
		14,9	**-81**	-10	71	**-83**	73
NRI	Czech Rep.	14,7	**-70**	-13	57	**-83**	70
AEKI	Hungary	5,5	**-49**	-25	24	**-83**	58
Prometey	Russia	2,8	**-103**	-39	64	**-83**	44
		2,9	**-103**	-15	88	**-83**	68
		5,6	**-103**	-34	69	**-83**	49
ORNL	USA	2,4	**-91**	-56	35	**-83**	27
JRC	EU		**-70**				
BARC	India		**-71**				
Mean			**-83**				

As it can be observed from the data, there is significant scatter in the $T_{41J\text{-}UN}$ as determined by the different laboratories. For the weld metal (Table 4.2), the values range from -40 to -62, with a mean value of -55ºC (see Figure 4.3), a typical amount of scatter expected for RPV weld metals, although quite small considering that the results are from eight different laboratories and the difference between maximum and minimum values is 22°C. However, for the base metal (Table 4.1) the scatter is very high with $T_{41J\text{-}UN}$ values from -49 to -103ºC and a mean value of -83ºC (see Figure 4.4).

Table 4.2. Summary of test results for WWER-1000 weld metal

Participants	Country	Fluence 10^{19} n/cm^2 E>0.5MeV	T_{41J-UN} ºC	$T_{41J-IRR}$ ºC	ΔT_{41J} ºC	$T_{41J-ADJ}$ ºC	$\Delta T_{41J-ADJ}$ ºC
Kuchatov Institute	Russia	5,2	**-53**	-3	50	**-55**	52
		6,5	**-53**	28	81	**-55**	83
		11,5	**-53**	89	142	**-55**	144
NRI	Czech Rep.	14,7	**-58**	97	155	**-55**	152
AEKI	Hungary	5,5	**-50**	16	66	**-55**	71
Prometey	Russia	2,8	**-40**	-2	38	**-55**	53
		5	**-40**	66	106	**-55**	121
ORNL	USA	2,4	**-62**	-28	34	**-55**	27
		8,8	**-54**	11	65	**-55**	66
JRC	EU		**-58**				
BARC	India		**-52**				
Mean			**-55**				

This amount of scatter is unusually high, especially given that all specimens were machined by the same institute and were taken from the same depth through the thickness (30 mm from a heat treated surface). Figures 4.1 and 4.2 show graphically the results of T_{41J-UN} reported by participants for the base and weld metals, respectively.

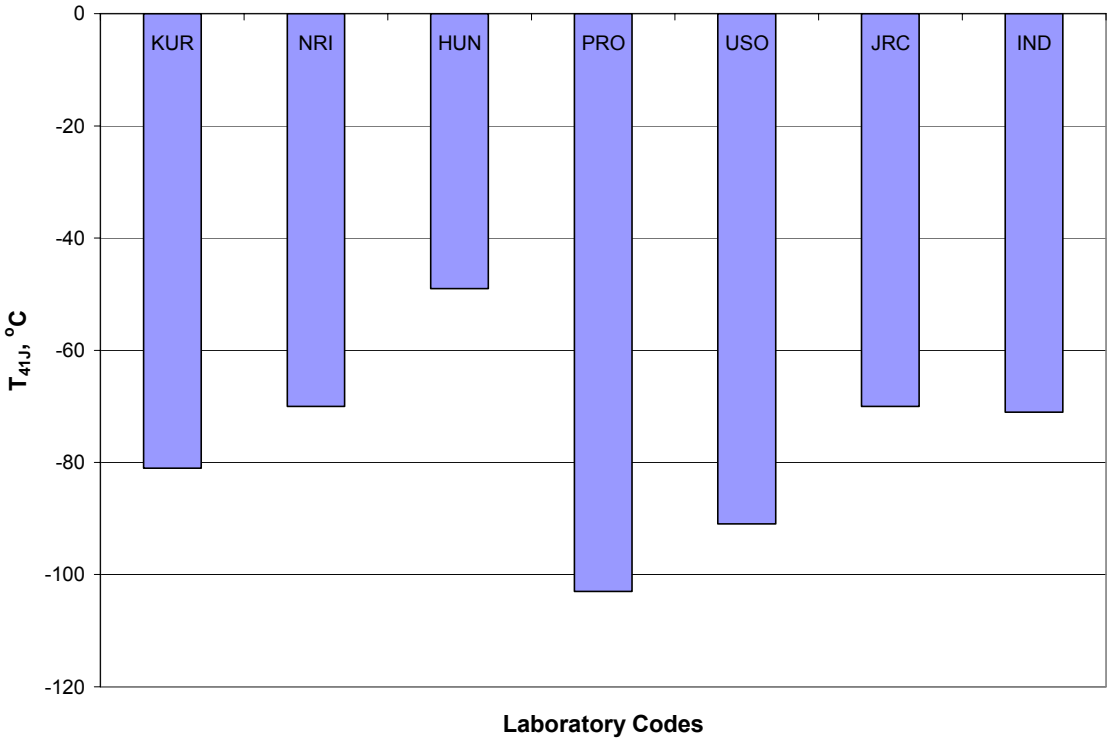

Fig. 4.1. Scatter in T_{41J-UN} as determined by individual laboratories for CRP WWER-1000 base metal.

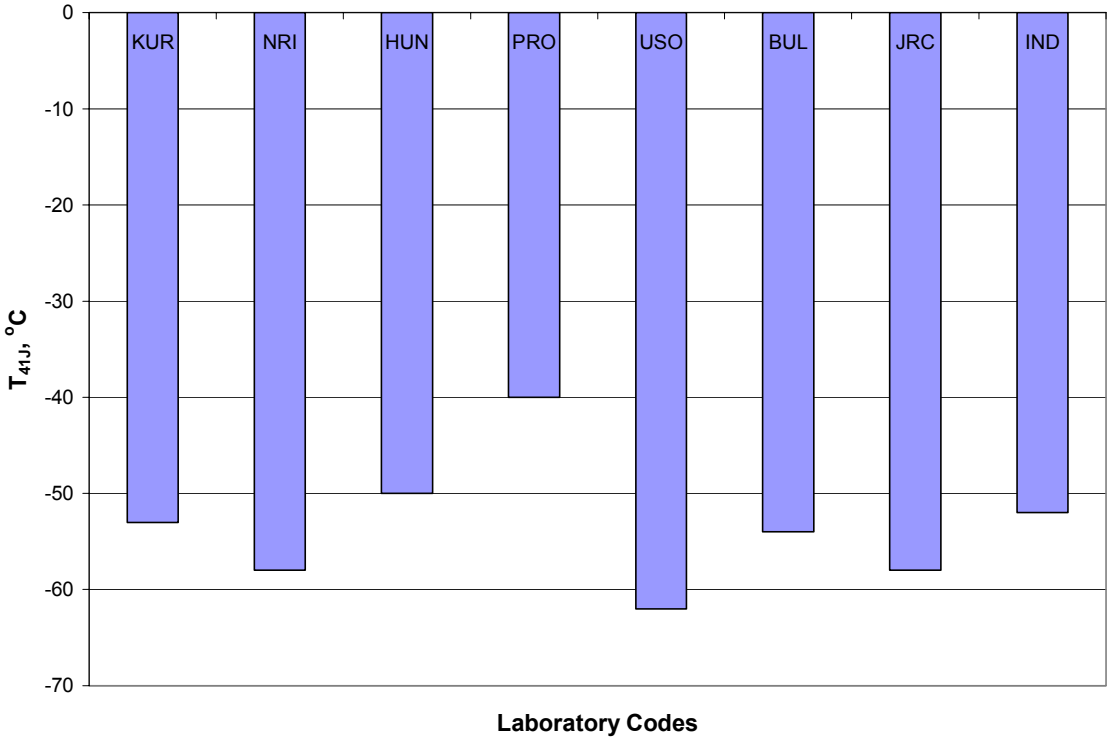

Fig. 4.2. Scatter in $T_{41J\text{-}UN}$ as determined by individual laboratories for CRP WWER-1000 weld metal.

Thus, the scatter of $T_{41J\text{-}UN}$ for base metal is significantly greater than that of weld metal. This result is in agreement with previous results showing relatively large scatter of Charpy impact parameters for base metal, albeit that this present result is greater than expected. However, the $T_{41J\text{-}UN}$ is rather low as expected for such material (the highest value is -49°C) and the mean value is shown as -83°C. Figures 4.3 and 4.4 show plots of all the Charpy impact energy data for the CRP WWER-1000 base and weld metals, respectively. Also, as shown, are hyperbolic tangent curve fits to each dataset with the lower shelf fixed at 3J.

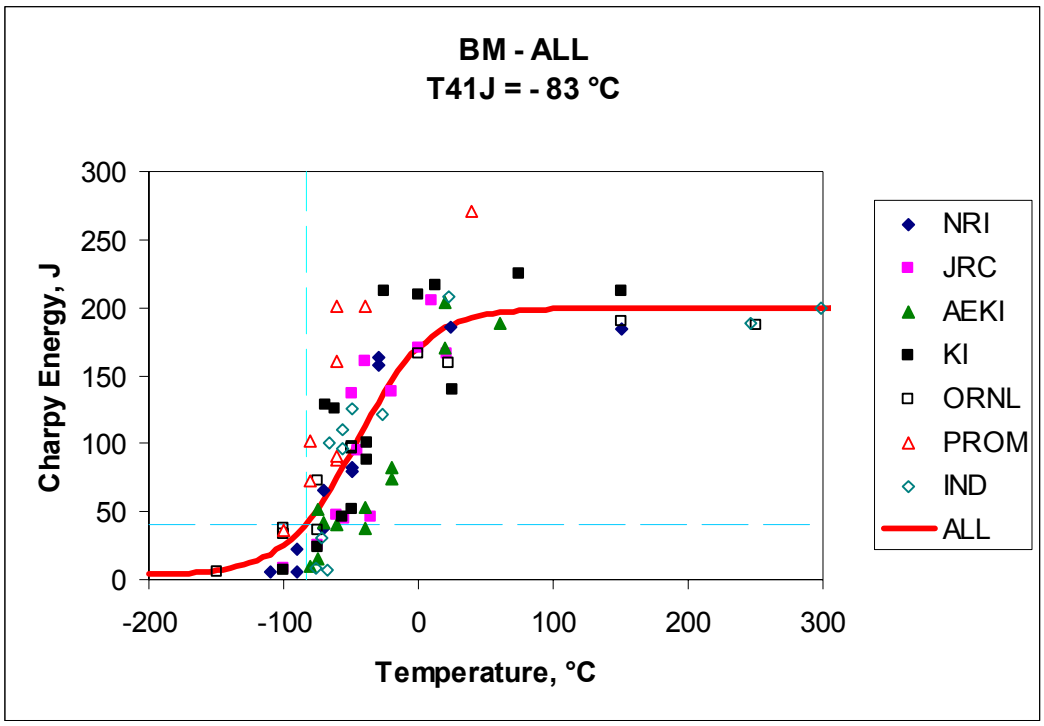

Fig. 4.3. Plot of all participants Charpy Energy vs Test temperature data for CRP WWER-1000 base metal with mean fit to data.

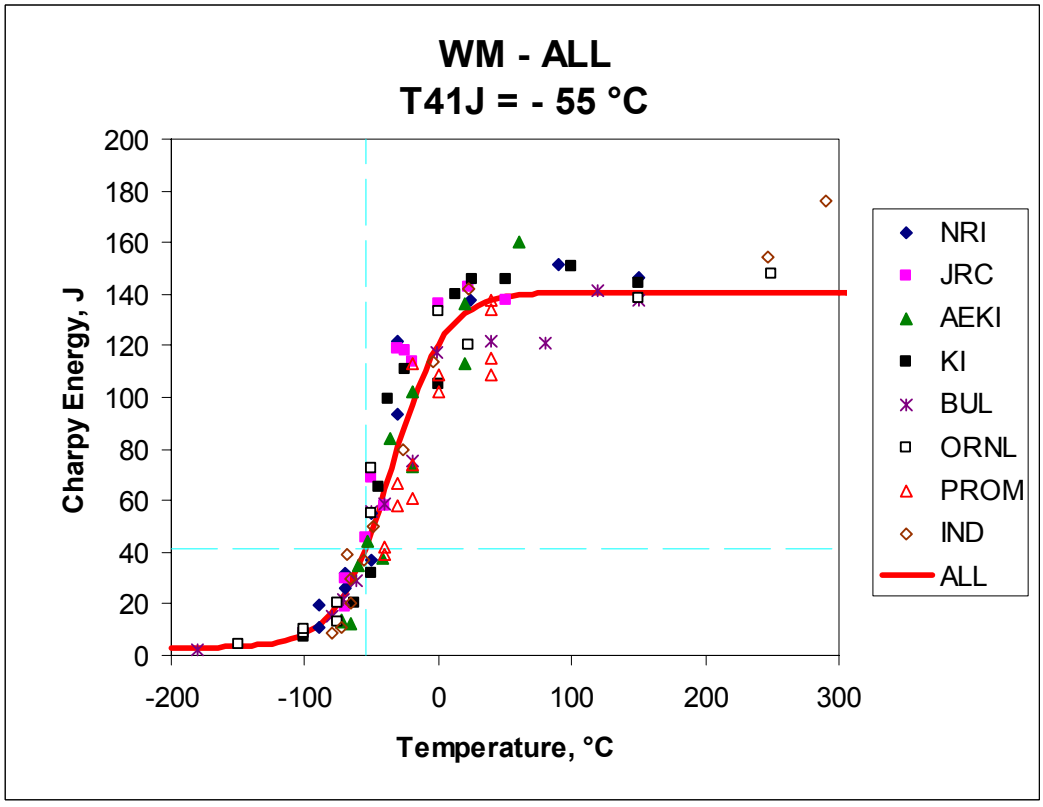

Fig. 4.4. Plot of all participants Charpy Energy vs Test Temperature data for CRP WWER-1000 weld metal with mean fit to data.

4.3. ANALYSIS OF IRRADIATION-INDUCED SHIFTS

As shown in Tables 4.1 and 4.2, an adjusted $T_{41J\text{-}UN}$ value ($T_{41J\text{-}ADJ}$) is given and is simply set equal to the mean value from all the participants results. Using the individual measured $T_{41J\text{-}UN}$ values obtained in the different laboratories and the relative shifts (ΔT_{41J}), Figures 4.5 and 4.6 show the dependence of shift versus fluence for the base metal and weld metal, respectively.

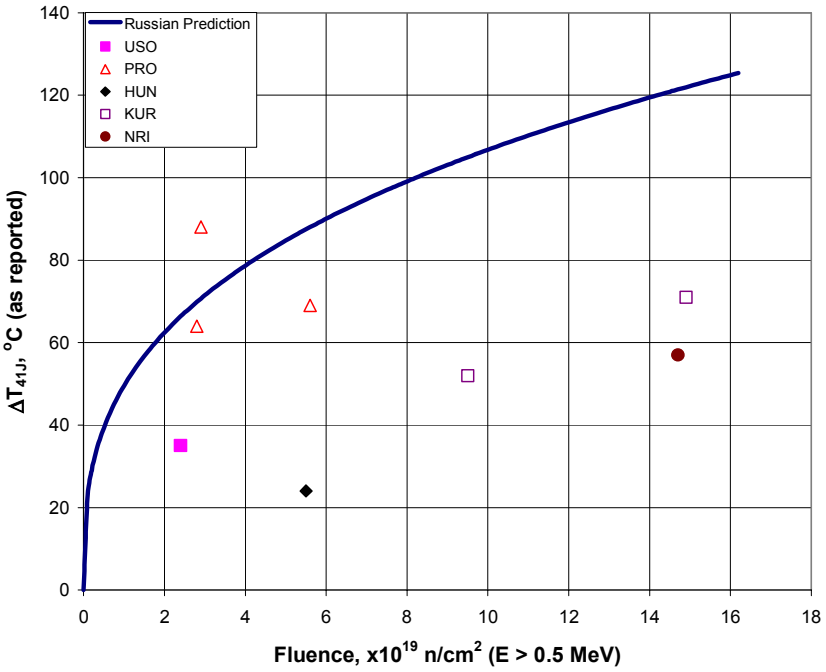

Fig. 4.5. Fluence dependence of ΔT_{41J} for WWER-1000 base metal (based on participants' $T_{41J\text{-}UN}$ values).

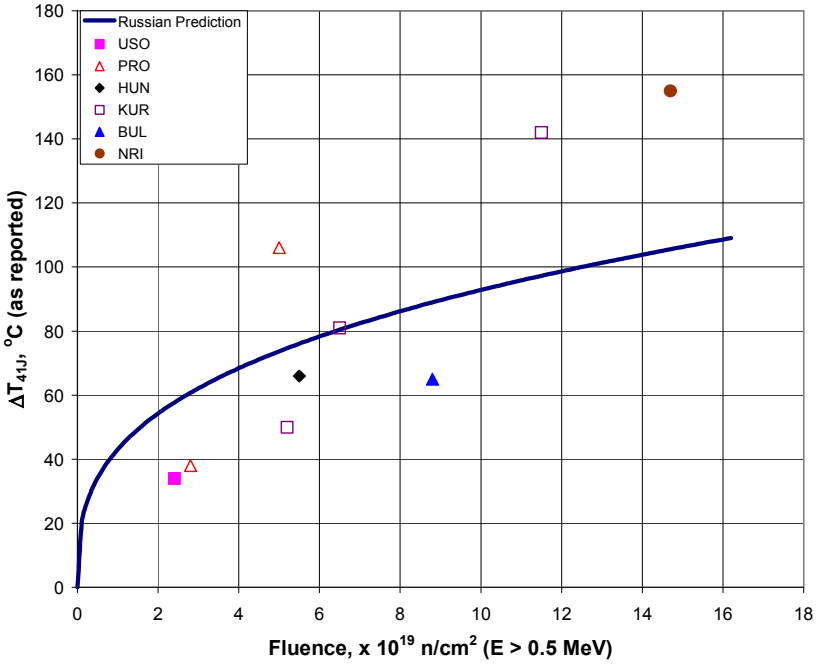

Fig. 4.6. Fluence dependence of ΔT_{41J} for WWER-1000 weld metal (based on participants' $T_{41J\text{-}UN}$ values).

The results in Fig. 4.5 for the base metal indicate no increase in embrittlement with fluence between about 3×10^{19} and 15×10^{19} n/cm^2 (>0.5 MeV), an unexpected result that is suspected to reflect the high degree of scatter in the measured values of $T_{41J\text{-}UN}$. In contrast, the weld metal, shown in Fig. 4.6, exhibited low scatter in $T_{41J\text{-}UN}$ and indicates a general increase of embrittlement with fluence.

To investigate the potential effect of the scatter in $T_{41J\text{-}UN}$ values, the mean $T_{41J\text{-}UN}$ ($T_{41J\text{-}ADJ}$) of the individual values obtained in the different laboratories was used to calculate an adjusted value of the irradiation-induced shift, $\Delta T_{41J\text{-}ADJ}$. The dependence of the adjusted shift on neutron fluence is given in Tables 4.1 and 4.2, and graphically in Figures 4.7 and 4.8 for the base metal (Ni=1.26 wt%) and weld metal (Ni=1.7 wt%), respectively.

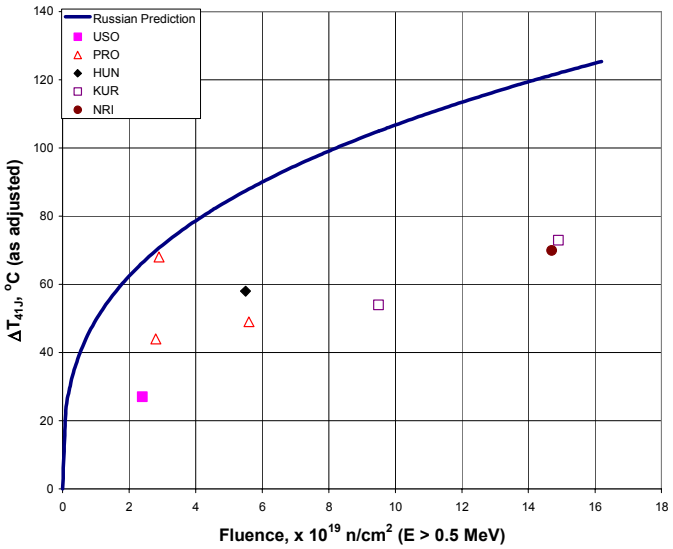

Fig. 4.7. Fluence dependence of $\Delta T_{41J\text{-}ADJ}$ for base metal (using $T_{41J\text{-}ADJ}$=-83 ℃).

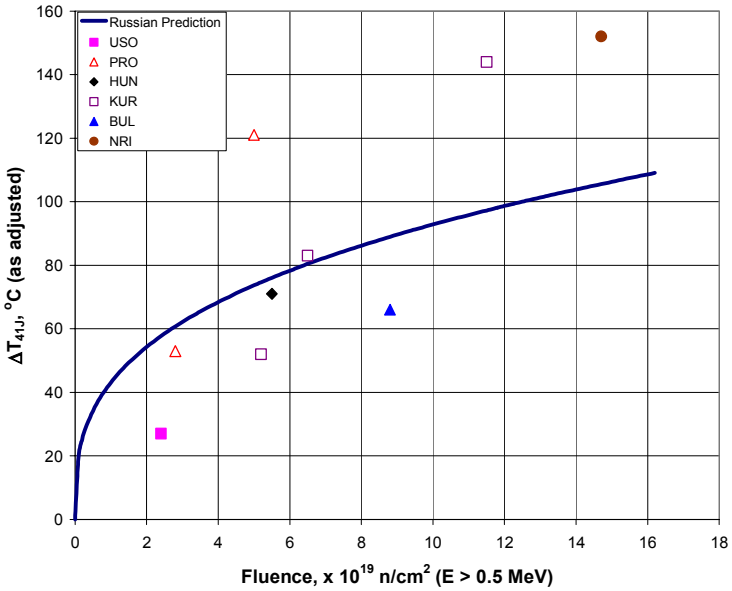

Fig. 4.8. Fluence dependence of $\Delta T_{41J\text{-}ADJ}$ for weld metal (using $T_{41J\text{-}ADJ}$=-55 ℃).

As it can be seen in Figures 4.7 and 4.8, the use of the mean $T_{41J\text{-}UN}$ considerably improves the fluence dependence for the base metal, decreasing the scatter. This is expected due to the use of a larger number of test data on such high scatter of $T_{41J\text{-}UN}$, see Figure 4.1. As for the weld metal, no significant improvement is observed, as expected, due to the small scatter in $T_{41J\text{-}UN}$ obtained in individual laboratories (see Figure 4.2).

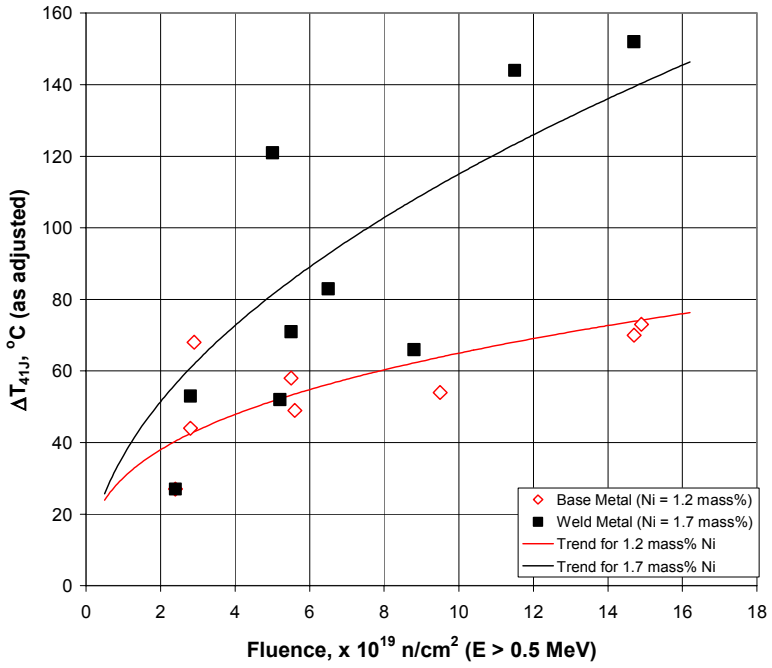

Fig. 4.9. Fluence dependencies of $\Delta T_{41J\text{-}ADJ}$ for WWER-1000 base and weld metals (using adjusted $T_{41J\text{-}ADJ}$ values).

Comparing the results shown in Figures 4.7 and 4.8, Figure 4.9 shows there is a clear effect of nickel and a clear delineation in embrittlement vs fluence between the base and the weld metals. Since the contents of copper and phosphorus are very low and practically identical in the two materials, the higher irradiation-induced embrittlement exhibited by the weld metal is attributed to its much higher nickel content, 1.7 vs 1.2 wt%. In spite of the substantial scatter for base metal data, the influence of nickel on the ductile-brittle transition temperature shift is definitive for these two materials.

4.4. RESULTS OF UPPER SHELF ENERGY MEASUREMENTS

The upper shelf energies before irradiation based on participants data are given in Table 4.3 and shown in Figure 4.10 for both base and weld metals. As shown in the table, the upper shelf energies vary from 125 to 175 J for the weld metal and from 180 to 270 J for the base metal, resulting in mean values of 200 J for the base metal and 140 J for the weld metal. In this case, significant scatter is observed for both materials.

Table 4.3. Upper shelf energy values based on participants data for CRP WWER-1000 base metal and weld metal

Laboratory Code	Base Metal USE J	Weld Metal USE J
BUL		130
NRI	185	146
HUN	196	160
IND	199	157
ECJRC-IE	192	143
KUR	213	145
PRO	270	127
USO	189	135

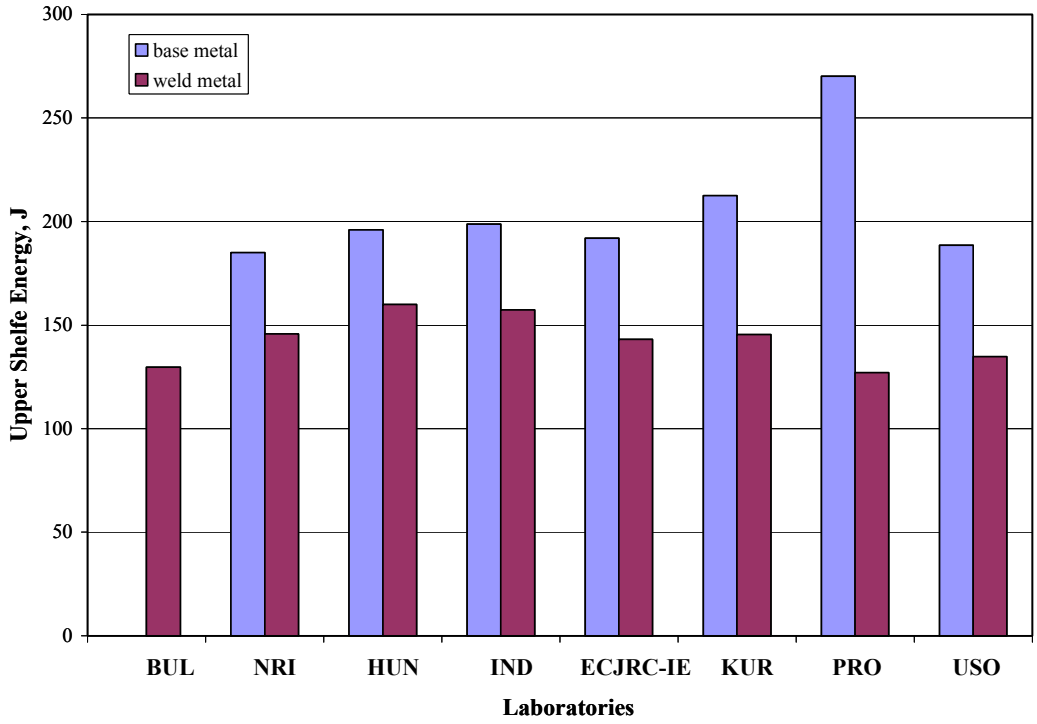

Fig. 4.10. Upper shelf energy in the unirradiated condition for both wwer-1000 base and weld metals (based on participants' charpy upper shelf energy data).

As shown in Tables 4.4 and 4.5, the unirradiated upper shelf energy values for both base and weld metals are the adjusted values based on the mean upper shelf energies from Figures 4.3 and 4.4. The upper shelf energies decreased following irradiation, as expected, in all cases but one as shown in Tables 4.4 and 4.5 and graphically in Figure 4.11.

Table 4.4. Irradiation-induced change in upper shelf energy values for CRP WWER-1000 base metal using mean upper shelf energy (see Fig. 4.3)

Laboratory code	Unirradiated USE (adjusted)	Irradiated		
		Fluence	USE	ΔUSE
	J	10^{19} n/cm^2	J	J
NRI	200	14.7	162	38
HUN	200	5.5	184	16
KUR	200	14.7	157	44
PRO	200	2.8	200	0
PRO	200	2.9	180	20
PRO	200	5.6	180	20
USO	200	2.4	194	6

Table 4.5. Irradiation-induced change in upper shelf energy values for CRP WWER-1000 weld metal using mean upper shelf energy (see Fig. 4.4)

Laboratory Code	Unirradiated USE	Irradiated		
		Fluence	USE	ΔUSE
	J	10^{19} n/cm^2	J	J
BUL	140	8.8	103	37
NRI	140	14.7	79	61
HUN	140	5.5	113	27
KUR	140	5.2	135	5
KUR	140	6.5	99	42
KUR	140	11.5	98	43
PRO	140	2.8	118	22
PRO	140	5.0	76	64
USO	140	2.4	145	-5

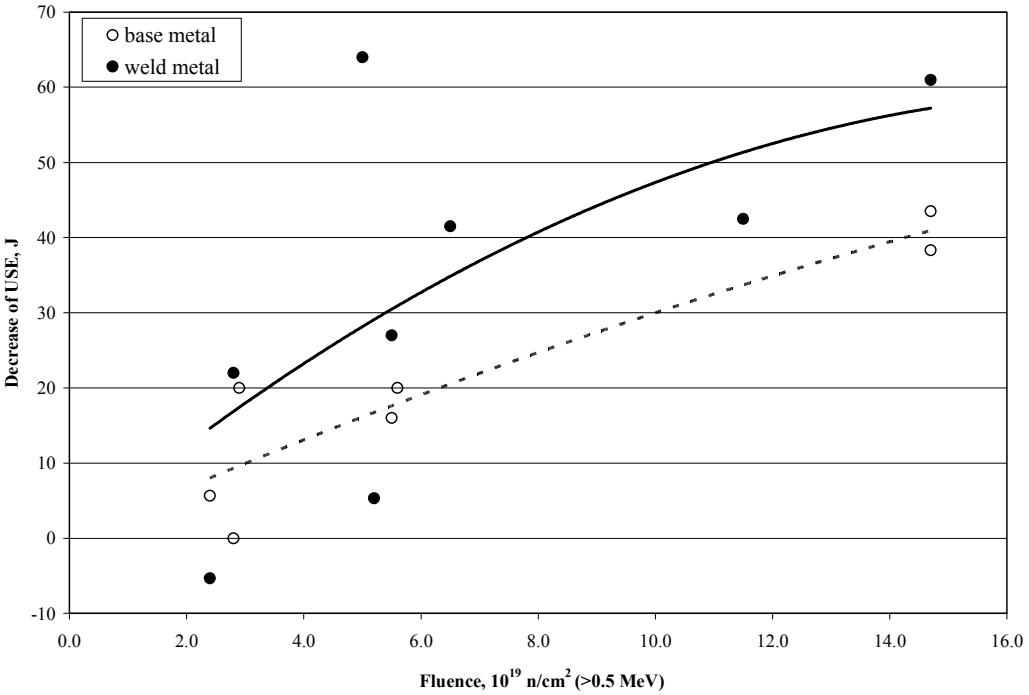

Fig. 4.11. Irradiation-induced upper shelf energy decrease vs fluence for WWER-1000 base and weld metals.

4.5. CORRELATION BETWEEN UPPER SHELF ENERGY DECREASE AND $\Delta T_{41J\text{-}ADJ}$

A graphical comparison between upper shelf energy decrease and $\Delta T_{41J\text{-}ADJ}$ is shown in Figure 4.12. A general trend of increasing upper shelf energy decrease with transition temperature shift is observed for both weld and base metals, as expected. Within the common range of data shown in Fig. 4.12, there appears to be little difference in the relationship between transition temperature shift and decrease in upper shelf energy.

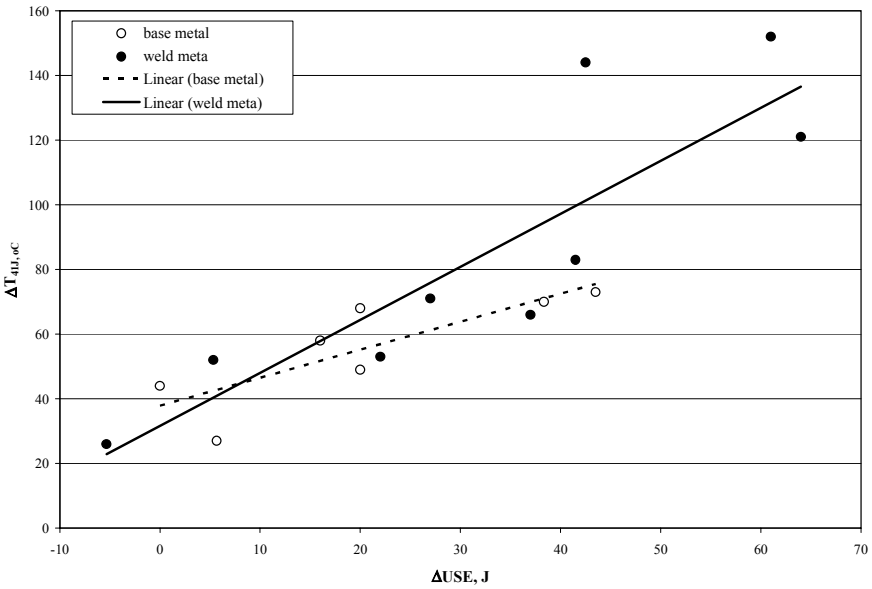

Fig. 4.12. Comparison between upper shelf energy decrease and $\Delta T_{41J\text{-}ADJ}$ for the irradiated WWER-1000 base and weld metals.

5. RESULTS FROM NATIONAL CONTRIBUTIONS

Many participants of the CRP performed investigations with so-called "national steels" in addition to the two mandatory WWER-1000 steels. In this chapter, the national steels will be discussed in two sections, one for WWER-1000 steels and the other for PWR steels. Note that microstructural studies are described in Chapter 6.

5.1. WWER-1000 NATIONAL STEELS

Table 5.1 lists the materials and contributions for the national WWER-1000 steels.

Table 5.1. WWER-1000 steels available from national contributions

Country/Lab	Contributions	Irradiations
PRO and KUR	Data on welds	MTR and WWER-1000
UKR	Similar material as used in CRP, previously irradiated. Surveillance data.	WWER-1000
JRC	Model alloys, high and low Ni	HFR-LYRA, Rovno and Kola NPPs
Germany (Special contribution)	Data collected on welds; not part of the CRP	MTR

5.1.1. MTR Results

From PRO and UKR reports, the effect of nickel is clearly observed for weld metal irradiated in a material test reactor; see Figure 5.1, where fluence is in units of 10^{19} n/cm^2, E > 0.5 MeV and the ductile-to brittle transition temperature shift, $DBTT_{shift}$, is in ^oC. By contrast, the results for a high Ni base metal as shown in Figure 5.2 show less embrittlement than for the welds in Figure 5.1.

5.1.2. Relevant model alloys results

Figure 5.3 shows data for model alloys irradiated at 270^{o}C at HFR-LYRA and the Kola NPP [5.1]. The results clearly show the strong effect of Ni in these materials.

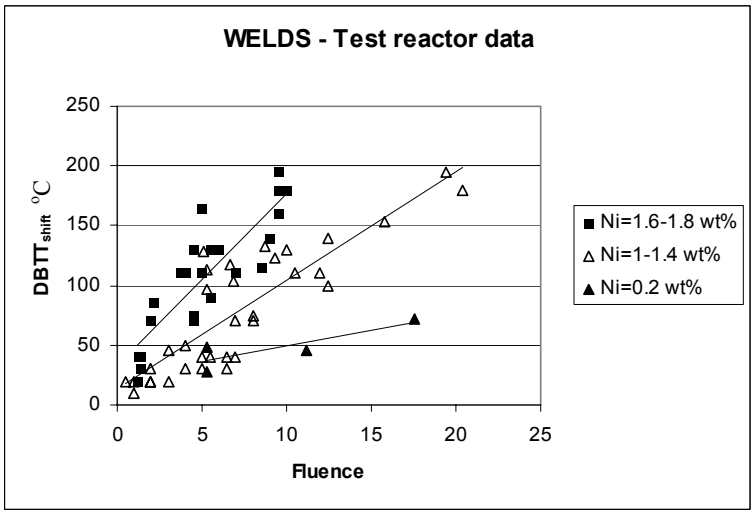

Fig. 5.1. Test reactor data for WWER-1000 welds showing the strong influence of nickel (fluence in 10^{19}, E>0.5 MeV).

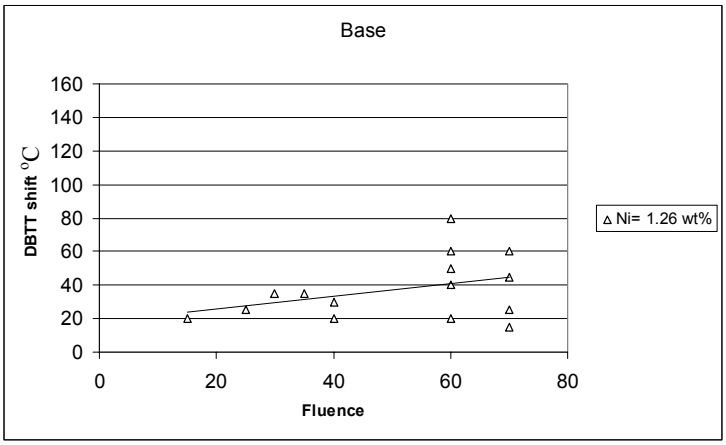

Fig. 5.2. Influence of nickel on base materials irradiated in MTR (fluence in 10^{19}, E>0.5 MEV).

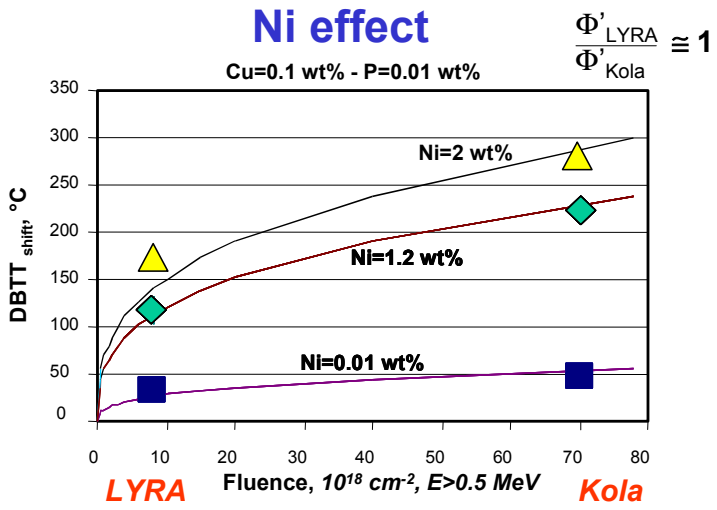

Fig. 5.3. Model alloy results illustrating the nickel effect.

5.1.3. WWER-1000 surveillance data

Several surveillance specimen sets of WWER-1000 RPV steels have been evaluated in Russia, Ukraine and Bulgaria by different testing organizations. These data have recently been re-evaluated [5.2]. These materials contain low and homogeneous levels of phosphorus and copper and significant variations of nickel and manganese. The observed temperature transition shifts due to irradiation show consistent behaviour and give an indication that Mn and Ni are the main contributors to embrittlement of such low Cu and P materials. Figure 5.4 illustrates this response to both nickel and manganese.

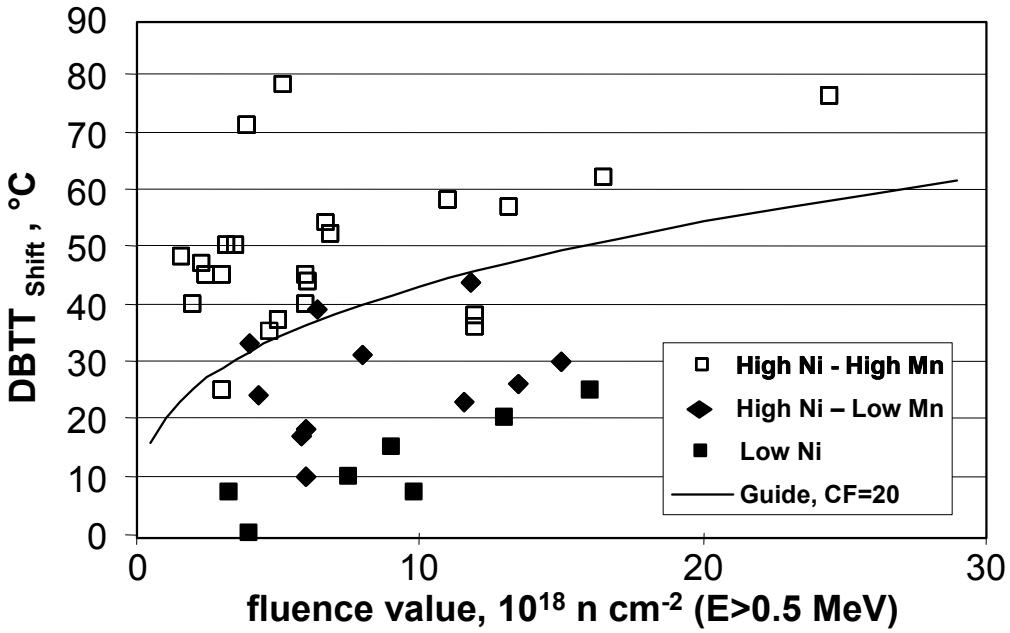

Fig. 5.4. Evaluation of surveillance data showing the influence of Ni and Mn.

Similar behaviour can be observed for high nickel content PWR welds (High Ni=1.7%, Low Ni=0.96%.).[1] Figure 5.5 illustrates the Langer data and shows the similar influence of Ni.

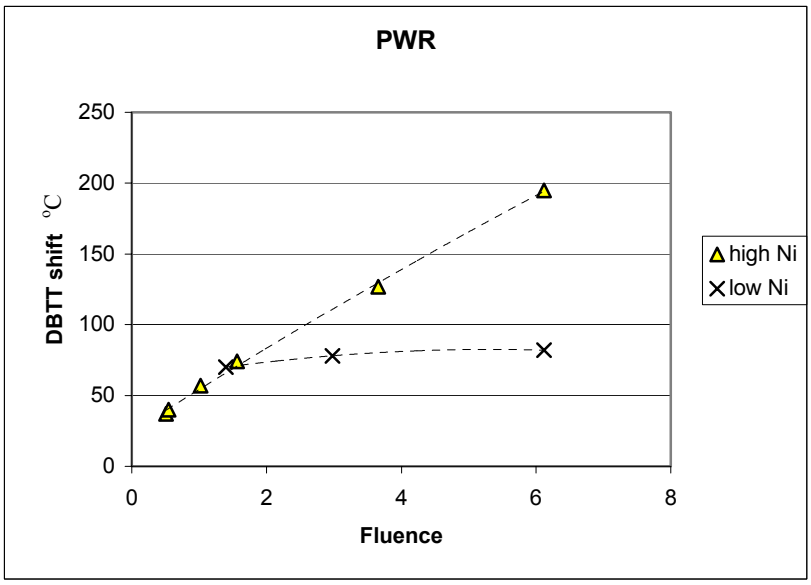

Fig. 5.5. PWR data from Langer showing similar effect of nickel as in WWER-1000 steels.

5.2. PWR NATIONAL STEELS

National steels have been evaluated for PWRs as reported by USO and USI. The steels and mechanical test results reported by USI are shown in Table 5.2. The steels include an A508 Grade 2 forging steel (typical of that used in the USA for commercial RPVs) in conjunction with a series of A508 Grade 4 steels. The primary feature of these A508 Grade 4 steels is the very high nickel content (as high as 3.5 wt%) as compared to the A508 Grade 2 or other PWR steels (or WWER-1000 steels). The effect of manganese was also an important

[1] These data were graciously provided by R. Langer, Framatome-ANP.

part of this study since the results show that the influence of high nickel is also affected by the amount of manganese in the steel. The results in Table 5.2 include fluence (ϕt in mdpa), flux (ϕ in mdpa/s), irradiation temperature (T_{irr} in ^{o}C), transition temperature shift at the 47 J level (ΔTT in ^{o}C), and irradiated Vicker's Hardness (VVN_{irr}). Note that the superclean alloy (Mn at 0.02 wt% and Cu at 0.03 wt%) shows very little embrittlement even with a nickel content of 3.53 wt%.

For the USO investigations by ORNL, the two National materials irradiated and tested have the chemical compositions given in Table 5.3. The primary elements of interest regarding radiation effects in these steels are nickel, copper, and manganese. As seen in the table, the nickel content is relatively high, while the copper content is also high. The manganese content is also higher in the KS-01 weld as compared with the A533B weld and much higher than for the WWER steels. Based on the chemical compositions, then, the two US National welds would be expected to be significantly more radiation sensitive than the two WWER-1000 materials. The KS-01 weld was produced by MPA, Stuttgart, with intentionally high contents of several elements, including copper, nickel, and manganese to ensure extremely high sensitivity to irradiation.

Table 5.2. Summary of materials, irradiation conditions, charpy shift, and hardness results

Steel	Ni	Mn	Cu	Si	ϕt mdpa	ϕ mdpa/s	Tirr (°C)	ΔTT (°C)	VHNirr
A508 Gr 2 ZV-806	0.59	0.59	0.12	0.26	85	~10^{-7}	~250	90	~240
A508 Gr4N 207N947	2.89	0.30	0.10	0.05	18	~10^{-4}	~240	68	~285
					79			165	~355
A508 Gr4N 123P171	3.75	0.29	0.08	0.03	68	~10^{-7}	~250	119	~310
A508 Gr4N 124S285	3.35	0.30	0.05	0.03	11	~10^{-7}	~265	0	~212
					17	~10^{-4}	~250	58	~245
Superclean 118K001	3.53	0.02	0.03	0.01	18	~10^{-4}	~250	21	~273
Weld	1.0	1.4	0.07	0.51	15	~10^{-4}	~240	~100	~300

Table 5.3. Chemical compositions for A533B and KS-01 weld materials investigated by USO (ORNL)

Material	**Chemical composition, wt %**									
	C	**Si**	**Mn**	**Cr**	**Ni**	**Cu**	**S**	**P**	**V**	**Mo**
A533B Weld*	0.11	0.183	1.271	0.04	1.204	0.197	0.017	0.014	0.003	0.546
KS-01 Weld	0.06	0.18	1.64	0.47	1.23	0.37	0.12	0.017	-	0.70

* NOTE: The values shown for the A533B weld are averages of three measurements in each case.

After neutron irradiation to a fluence of $0.8x10^{19}$ n/cm^2 (E > 1 MeV), corresponding to $1.38x10^{19}$ n/cm^2 (E > 0.5 MeV), the KS-01weld exhibited:

- Charpy T_{41J} shift of 169^{o}C,
- Reasonable comparison with predicted value from USNRC Regulatory Guide 1.99, Rev. 2 [5.3] of 162^{o}C, but an over-prediction from a correlation by Eason et al. [5.4] of 186^{o}C.
- Decrease in upper shelf energy (USE) from 124 J to 78 J.
- Increase in yield strength from 600 to 826 MPa.
- Shift in fracture toughness transition temperature (T_0) of 160^{o}C.
- The Master Curve shape was followed except at the highest temperature for the irradiated case where low toughness brittle fractures occurred at temperatures further above T_0 + 61^{o}C with a leveling of the K_{Jc} data from the Master Curve shape concept.

For the A533B weld irradiated to a fluence of $1.38x10^{19}$ n/cm^2 (E > 1 MeV), corresponding to $2.37x10^{19}$ n/cm^2 (E > 0.5 MeV), the Charpy transition temperature results showed the following:

- Charpy T_{41J} shift of 102°C.
- Comparison with predicted value from USNRC Regulatory Guide 1.99, Rev. 2 of 154^{o}C is overly conservative, and similarly an over-prediction for the Eason et al. correlation prediction of 137^{o}C; also the prediction using ASTM E900-02 [5.5] is identical to the Eason et al. prediction.

Thus, the mechanical property tests show some significant embrittlement for the two high Ni welds, but the most recent predictive formulas [5.4, 5.5] produce higher estimates of embrittlement than those measured in both cases. The fracture toughness shift (ΔT_0) measured for the KS-01 weld is very close to the measured ΔT_{41J} Charpy shift.

REFERENCES

[5.1] DEBARBERIS, L., TÖRRÖNEN, K., SEVINI, F., ACOSTA, B., KRYUKOV, A. AND NIKOLAEV, Y., "Experimental Studies of Copper, Phosphorus and Nickel Effect on RPV Model Alloys at Two Different Fluences"; Proceedings of Workshop on RPV Life Predictions, Madrid, Spain (2000).

[5.2] KRYUKOV, A., ERAK, D., DEBARBERIS, L., SEVINI, F., AND ACOSTA, B., "Extended Analysis of VVER-1000 Surveillance Data", International Journal of Pressure Vessel and Piping, Vol. 79, (2002) 661–664

[5.3] U.S. NUCLEAR REGULATORY COMMISSION, Regulatory Guide 1.99 Revision 2, "Radiation Embrittlement of Reactor Vessel Materials," Office of Nuclear Regulatory Research, U.S. NRC, Washington, DC, USA (1998).

[5.4] EASON, E.D., WRIGHT, J.E. AND ODETTE, G.R., "Improved Embrittlement Correlations for Reactor Pressure Vessel Steels", NUREG/CR-6551, U.S. Nuclear Regulatory Commission, Washington, DC, USA (1998).

[5.5] AMERICAN SOCIETY FOR TESTING AND MATERIALS, "Guide for Predicting Radiation-Induced Transition Temperature Shift in Reactor Vessel Materials, E706 (IIF)," ASTM E 900, Annual Book of ASTM Standards, Vol. 12.02, American Society for Testing and Materials, West Conshohocken, PA. USA (2002).

6. MICROSTRUCTURAL EVALUATIONS

6.1. INTRODUCTION

In most cases, the understanding of irradiation embrittlement behaviour of low alloy reactor pressure vessel steels is based on the measurement of mechanical property changes (Charpy V-notch ductile-brittle transition temperatures or yield strength increases) for steels that have been irradiated under a range of different conditions (neutron fluence/flux and temperature). Based on these mechanical test data alone, it often is not possible to explain observed results for these steels with respect to sometimes apparently conflicting data from other sources.

However, by understanding the mechanism of irradiation damage in these materials, it is possible to address key issues that mechanical testing alone cannot explain. One germane example is the role of Ni in creating damage under irradiation conditions. The terminology irradiation embrittlement (or damage) is used to describe the overall degradation in material caused by neutron irradiation. This embrittlement includes the degradation in fracture toughness and the increase in material hardness caused by irradiation, as well as the formation of vacancy- and solute-type defects within the microstructure resulting from neutron irradiation exposure.

The fundamental approach of any program focused on understanding irradiation embrittlement should be to identify physical changes in the microstructure caused by neutron irradiation using state-of-the-art analytical techniques and to correlate these changes with the observed changes in mechanical properties. By understanding how the irradiation-induced microstructure develops, it is possible to evaluate the mechanical performance of reactor pressure vessel steels after irradiation and to describe the irradiation embrittlement process.

There are published data that demonstrate significant degraded behaviour of reactor pressure vessel steels with elevated levels of Ni. The first source is WWER-1000 steels with Ni contents up to 1.9 wt% in base metals and 2.5 wt% in weld metals [6.1]. Also, published data on Rolls Royce welds with Ni contents up to 1.7 wt% show significant degraded behaviour [6.2]. Studies on model alloys with varying Ni contents (up to 1.6% Ni) conducted at the University of California at Santa Barbara (UCSB) [6.3] have identified an increase in irradiation-induced hardening with high Ni levels in steels. Another model alloy study conducted at the Joint Research Centre has produced additional data showing the embrittling nature of Ni [6.4]. Additionally, analyses of surveillance program databases in several Western countries have shown a synergistic effect between Ni and Cu content for their country-specific reactor pressure vessel steels [6.5. 6.6].

These findings have led to a negative perception in the nuclear industry for the use of high Ni steels in reactor applications. Accordingly, it would be expected that low alloy steels containing very high Ni levels (such as A508 Grade 4 steel with Ni at about 3.3 wt%) would exhibit significantly increased irradiation damage. However, mechanical property data on high Ni, A508 Grade 4 steels have shown comparable results as for lower Ni, A508 Grade 2 steels (Ni less than about 0.9 wt%) [6.7]. This behaviour can only be explained if the mechanisms by which irradiation embrittlement occurs are better understood and the role of alloy chemistry is quantified more explicitly. It has recently been shown that the enhanced embrittling effect of Ni is complex and involves other elements. For high quality A508 Grade 4N steels, the effect of Ni is only important if the Mn content is at the nominal level of 0.3 wt%; in superclean cases where the Mn level is very low (about 0.02 wt%), Ni has very

little effect in terms of creating a precipitate microstructure or a deleterious effect on mechanical properties [6.8].

6.2. MICROSTRUCTURAL TECHNIQUES AND STUDIES

The first phase of a typical irradiation damage mechanism program is to scope the range of steels and irradiation conditions to define key materials to characterize. Additionally, the suitability of candidate analytical techniques must be established for the characterization and documentation of the complex microstructural changes developed during neutron irradiation. A first step is to look for solute-related features that can be identified in irradiated steels using three-dimensional atom probe field ion microscopy (3D-APFIM). Solute features that can be inferred from 3D-APFIM refer to a range of obvious solute-rich *precipitates* to smaller *clusters* to statistically significant non-random distributions of solute atoms within the matrix that can be called *embryos, atmospheres, or fluctuations*. Studies using small-angle neutron scattering (SANS) can also be helpful in defining the size and volume densities of solute features. The use of these two techniques allows a more thorough understanding of the microstructure changes since the results from both are complementary; in fact, the consistency of results achieved using both techniques provides further confidence in the results obtained.

To go beyond the solute-related damage to also include matrix damage, which is typically vacancy related, other techniques are required. The effects of neutron fluence rate and other elemental interactions may be manifested in the vacancy-related embrittlement. Key state-of-the-art combined techniques are positron annihilation (PA) and Vickers hardness (VH) tests, often utilizing post-irradiation annealing (PIA) as a means to separate the temperature range of the damage mechanisms. The PA approach can be of several types: PA lifetime and PA lineshape analysis (PALA).

The PALA can be characterized by different methods such as Doppler broadening and PA angular correction (providing measures of S and W parameters). The use of a pulsed low energy positron system (PLEPS) can also yield additional insight into the positron lifetime spectrum. The use of 3D-APFIM data combined with PA and hardness data obtained as a function of PIA treatment can allow the separation of embrittlement into the two hardening contributions, vacancy- and solute-related hardening.

Each microstructural evaluation technique provides specific information that complements the information generated by the other techniques, thereby providing a unique perspective for characterizing the solute-related hardening features and vacancy-related matrix damage induced by neutron irradiation. There are other techniques that can be applied to further enhance and complement the data obtained from 3D-APFIM, SANS, and PALA-hardness (utilizing PIA where possible). One of these techniques is Mössbauer spectroscopy (MS), which can provide complementary information to the PALA results. One other technique that can be utilized for the evaluation of irradiated microstructures is internal friction, but this type of information was not used in the studies conducted in this program. Of course other measures of microstructure can be performed, including simple light optical microscopy, scanning electron microscopy (SEM), and transmission electron microscopy (TEM), but these methods do not have the resolution capability to study the type of solute- and vacancy-related defects found in irradiated reactor pressure vessel steels.

Microstructural evaluation of both the program WWER-1000 steels and some limited national steels (primarily from the US) have been performed. These evaluations are discussed next.

6.3. MICROSTRUCTURAL STUDIES ON HIGH NICKEL STEELS

Even though the title of this CRP includes mechanisms of a nickel effect on embrittlement after irradiation, only a limited amount of microstructural work was performed on WWER-1000 steels. The mechanical property changes for the CRP WWER-1000 base and weld metal have been reported earlier in this document. 3D-APFIM examinations were performed by USO — Oak Ridge National Laboratory (ORNL) — for non-irradiated WWER-1000 materials and specimens irradiated at the Ford Nuclear Reactor by ORNL (see Chapter 3) and for U.S. national materials as described in Chapter 5. PA examinations were performed by SLO — the Slovak University of Technology — on non-irradiated WWER-1000 materials and specimens irradiated in the NRI in the Czech Republic (see Chapter 3). 3D-APFIM, SANS, and PALA-hardness using PIA methods were used to describe the microstructure of some U.S. national steels by USI containing higher levels of Ni than in WWER-1000 steels. Some non-irradiated examinations were performed by BUL — the Institute of Metal Science in Bulgaria — on the WWER-1000 weld metal used in this project. A summary of all of these results are presented next.

6.3.1. 3D-APFIM examination of WWER-1000 steels – USO

Atom probe tomography (APT), which is another name for a type of 3D-APFIM, was conducted for the two WWER-1000 base metal and weld metals in the post-irradiation condition. Figures 6.1 and 6.2 show the atom maps for the two WWER materials. The atom map for the forging steel (Figure 6.1) shows that P, Ni, and Si segregated to a dislocation and a low number density of ultra-fine Ni- and Mn-enriched precipitates were created after irradiation to a fluence of 1.4 x 10^{19} n/cm^2 (E >1 MeV), 2.4 x 10^{19} n/cm^2 (E > 0.5 MeV). The two materials were irradiated at the Ford Nuclear Reactor at a temperature of 288ºC and at a flux of about 7×10^{11} n/cm^2·s (E > 1 MeV), 12×10^{11} n/cm^2·s (E > 0.5 MeV). The irradiated weld metal (Figure 6.2) shows ultra-fine Mn-, Ni-, and Si-enriched precipitates even though the measured Charpy shift at 47 J was only 34^{o}C. Note that no significant copper enrichment was observed in any of the precipitates. The APT analysis of the WWER-1000 weld and base metal have revealed ultra-fine precipitates or “embryos” of irradiation-induced precipitates given that the irradiation fluence for these two materials was relatively low.

6.3.2. 3D-APFIM examination of US National steels – USO

APT was conducted for two US national steels (KS-01 and an A533B weld) in the post-irradiation condition. The bulk Ni and Cu content for the two welds was: 1.23 wt% Ni and 0.37 wt% Cu for the KS-01 weld, and 1.20 wt% Ni and 0.20 wt% Cu for the other A533B weld. In the APT analysis of the KS-01 weld, the atom maps shown in Fig. 6.3 reveal irradiation-induced precipitates enriched in Cu, Mn, Ni, P, and Si. Moreover, they reveal that irradiation produced an extremely high number density of precipitates, significantly higher than other RPV steels irradiated to similar or higher fluences; the KS-01 weld was irradiated to a relatively low fluence of 0.8 x 10^{19} n/cm^2 (E > 1 MeV) at 288°C in the Ford Nuclear Reactor, but the transition temperature shift was 160^{o}C in terms of fracture toughness (ΔT_0) and 169^{o}C in terms of Charpy properties (ΔT_{41J}).

The APT data analysis reveals the three-dimensional nature of the precipitates. The atoms that comprise each precipitate are identified with the maximum separation method. This method is based on the principle that the solute atoms in a solute-enriched precipitate are closer together than those in solid solution in the surrounding matrix. The images in Fig. 6.4

show the approximately spherical morphology of the precipitates. The data analysis also can reveal the elemental concentration distribution relative to the precipitate center. The plots in Fig. 6.5 show that copper is concentrated at the core of the precipitate, that manganese has a more extensive profile into the matrix, and the nickel is more associated with the interface.

Data analysis can also be used to estimate the composition of each nano-scale precipitate with use of the envelope method, the results of which can then be used to estimate the enrichment of each element relative to the matrix concentration. This analysis gives enrichment factors of 89 for copper, 29 for nickel, 24 for manganese, and 2.7 for silicon. The APT analysis of KS-01 also showed that diffuse phosphorus clusters were formed in this material as a result of irradiation and were approximately 3 nm in extent, although the number density was approximately 50 times lower than that for the Cu-enriched precipitates. In addition to the phosphorus clusters formed in the matrix, some phosphorus segregation to dislocations was also observed.

APT results from the other A533B weld metal (submerged arc process) with higher Ni but lower Cu at a fluence of 1.4 x 10^{19} n/cm^2 (E > 1 MeV) exhibited a high number density of ultrafine Cu-, Mn-, Ni- and Si-enriched precipitates. The T_{41J} shift was 102ºC at this fluence. Phosphorus segregation was also observed on dislocations. These observations support other studies that have shown a strong synergism of nickel and manganese in increasing radiation sensitivity of RPV steels.

6.3.3. PA and MS examinations of WWER-1000 steels – SLO

In the non-irradiated condition, both the WWER-1000 base and weld metals were examined using the PA lifetime approach. The results indicate the possibility that the base metal has less vacancies or vacancy clusters than the weld metal. Small differences (but almost in range of statistical error) were observed in measurements using backscattering Mössbauer spectroscopy (MS). Slightly higher content of alloying elements in the weld metal (mainly Mn, Mo and/or Ni) could cause a measurable difference as seen in MS relative to the contribution of the alloying elements positioned near iron atoms in the lattice structure.

Other studies on the model alloys described in Chapter 5 were conducted to simulate the differences in WWER-1000 materials with varying elemental contents. It was found that the positron lifetime increases by increasing the Cu concentration at low levels of Ni. However, at higher levels of Ni (up to 2 wt%) increasing the Cu content does not substantially influence the positron lifetimes. Even though the changes in P content tend to be small, increasing P content results in an increase in the positron lifetime. This effect can be rationalized as a contribution of P due to the strain of interstitial atoms on the lattice structure evident in the material microstructure. The increase of the lifetime with Ni content was predominant at all levels of Cu.

Specimens from the CRP WWER-1000 base and weld metals, and a WWER-440/213 weld metal (105khMFT steel with essentially no Ni), were irradiated in the experimental reactor at NRI Řež. The WWER-1000 steels were irradiated to a fluence of 4 x 10^{23} n-m^{-2} (>0.5 MeV) at a temperature of 290±10°C. The specimens were polished to a mirror-like finish for PLEPS analysis. The WWER-440/213 weld metal specimens with no Ni were irradiated in a nuclear power plant WWER-440 irradiation channel to a fluence of 1.25 x 10^{24} n-m^{-2} (>0.5 MeV) at a temperature of 275±5°C. All of the specimens were measured using PLEPS in three states: the as-received state, after irradiation, and after a post-irradiation heat treatment of 2 hours (in a vacuum) at 475°C. Results from the PLEPS measurements suggest

that the WWER-1000 weld metal with the highest Ni content has the worst microstructure, and the no-Ni weld metal (WWER-440/213) has the best microstructure. The parameter mean lifetime increases with the density of vacancy-related defects (mono-vacancies, di-vacancies, open volume defects, Frenkel pairs and/or dislocation lines). The WWER-1000 weld metal has a higher content of alloying elements in comparison to the WWER-1000 base metal including both a higher content of Ni (1.7 to 1.26 wt%), as well as a higher content of Mn (0.73 to 0.46 wt%). After irradiation, the WWER-1000 base metal shows relatively better resistance against irradiation in comparison to both weld metals. Remarkable is the strong increase of mean lifetime for the WWER-44/213 weld metal. After post-irradiation heat treatment, the mean lifetime parameter recovers back to the values in the as-received state. Thus, almost all defects caused by irradiation were annealed out.

The absolute mean lifetime values are relatively high. For an ideal steel without any defects, the mean lifetime should be about 120 ps. For pure iron, the mean lifetime should be about 110 ps. The mean lifetime values measured were 140–150 ps, which indicate that some defects were created during the fabrication process.

Additionally, the TRIM (the Transport of Ions in Matter) computer program was used to simulate the results for an idealized steel alloy with a composition of 94% iron, 4% chromium, and 2% nickel. The model considers linear collision if an atom in turn collides with only stationary atoms in the target, and never with atoms that have already been set in motion by a previous event (as shown in Fig. 6.5). In a related study, an ab-initio investigation was conducted, based on local density approximation functional theory with the aim to explain the role of nickel on pressure vessel steel properties. It was shown that increasing the concentration of nickel in an iron lattice controls the hardening effect in vessel steel in good agreement with experimental observations. On the other hand, the computational model shows a trend of Ni in an iron lattice to increase the concentration of nonbonding electrons. Since these electrons are positioned in partially filled Ni-d bands, a related part of electronic charge may increase the radiation sensitivity of highly Ni-alloyed steel.

6.3.4. 3D-APFIM, SANS and PALA-Hardness (Post-irradiation annealing) examinations of high Ni content US and WWER steels – USI

Studies were conducted on much higher Ni steels than typically used in commercial PWRs or WWER vessels — see Table 5.1. A combination of microstructural techniques was used to characterize the irradiation-induced microstructure of low Cu content A508 Grade 4N forging steels. The microstructural techniques used were 3D-APFIM, SANS, and PALA.

One key result from these studies was that Mn is a significant solute in the development of hardening and co-segregation during neutron irradiation of A508 Grade 4N steels. Mn is also involved in the formation of both cluster embryos and precipitates in these high Ni, low Cu steels. Mn distributions become increasingly non-random, and Mn tends to co-segregate with Ni during neutron irradiation, despite the relatively low levels of Mn (and Cu) in these steels. These non-random features lead to a distinct irradiation-induced hardening component that remains even after PIA. In the absence of Mn (such as in a “superclean” A508 Grade 4N), no such solute-related hardening component was detected.

Hardness data have confirmed published observations that irradiation-induced hardening for high flux irradiations is directly proportional to transition temperature shift. Solute-related hardening features develop under both high flux and low flux irradiation in A508 Grade 4N materials. Solute “fluctuations” develop first and co-segregation leads to formation of diffuse,

ultra-fine solute-enriched clusters or embryos. Well-defined solute-rich "precipitates" were detected following irradiations under low flux conditions to high fluence.

Whereas high flux irradiations promoted both vacancy-related and solute-related hardening, low flux irradiation (at ~30ºC higher temperatures) appeared to promote predominantly solute-related hardening in A508 Grade 4N steels. Thus, vacancy-related damage appears to anneal out over long periods of time at the irradiation temperature for these low Mn steels. SANS appears to detect vacancy-related damage and more distinct solute-related features, but not solute "fluctuations."

The SANS results of WWER materials investigated in [6.9] provide qualitatively similar irradiation-induced defect cluster size distributions. The defect content as function of irradiation dose is shown in Fig. 6.8. If the two types of WWER base metal are separated, approximately linear trends of Δc versus dpa are observed. WWER 1000-type steels have a higher sensitivity to irradiation-induced defect clustering than WWER 440-type steels. A special case is the WWER-1000 weld metal, which has an extremely high sensitivity.

In summary, two contributions to the observed irradiation-induced hardening have been identified for high flux irradiation conditions: (1) solute-related hardening features (Mn and Ni solute fluctuations); and (2) vacancy-related matrix damage. 3D-APFIM and SANS characterization of post-irradiation annealed specimens confirmed that the Mn and Ni solute fluctuations contributed to the observed irradiation-induced hardness of the steel. Furthermore, characterization of the 3.5 Ni – 0.02 Mn superclean steel demonstrated that no stable solute-related hardening occurred during neutron irradiation. Therefore, Mn has a significant effect on the development of solute-related hardening features formed during neutron irradiation and the observed irradiation damage behaviour of high Ni low alloy steels. In addition, comparison of low flux and high flux irradiated steel revealed that the magnitude of solute-related hardening were similar, despite nearly three orders of magnitude difference in flux. However, negligible vacancy-related damage was detected in the low flux irradiated steel. SANS results of both WWER-440 and WWER-1000 steels exhibited similar results, with the WWER-1000 weld metal showing an extremely high sensitivity to irradiation-induced defect clustering.

6.3.5. Optical, SEM, and TEM examination of coarse microstructure of WWER-1000 weld metal – BUL

Light microscopy, scanning electron micrscopy (SEM), and transmission electron miscroscopy (TEM) were used to characterize the WWER-1000 weld metal. The macrostructure was shown to reveal distinct boundaries between the welding passes. As expected, no differences in macrostructure were observed between irradiated and non-irradiated weld metal.

The microstructure studies revealed that there were fan-like zones of lower bainite — lath-shaped with carbides arranged along lath boundaries. The shape of carbides was rod-like of length up to 300 nm. In some areas, the laths of bainite were very narrow with almost no carbides at the boundaries indicating some martensite. Fine needles of Mo_2C were precipitated along <011> planes in the ferrite matrix; a small quantity of very fine spherical precipitates (up to 5 nm) was randomly distributed in the matrix. Irradiation did not affect the Mo_2C precipitates. The size of the spherical precipitates remained unchanged, although the quantity appeared to be higher in the irradiated condition. No dislocation loops could be observed.

The SEM studies were conducted on broken Charpy specimens. All upper shelf specimens (both irradiated and non-irradiated) exhibited ductile dimple rupture. Lower shelf specimens show transgranular cleavage facets. There is mixed mode behaviour in between the lower and upper shelves. In both the unirradiated and irradiated conditions, some intergranular facets were observed; these facets were usually elongated and arranged in parallel rows. This type of fracture appears to be due to crack propagation along the boundaries of dendrite crystallites. It was not possible to quantify any differences after irradiation.

6.4. INFERENCE RELATIVE TO EMBRITTLEMENT MECHANISMS

The current view of radiation embrittlement of pressure vessel steels is focused on three main mechanisms: matrix hardening, solute precipitation hardening, and intergranular loss of cohesion due to segregation of elements such as phosphorus to grain boundaries. Nickel has a definite effect in increasing embrittlement in conventional PWR and WWER steels. The role of nickel appears to be synergistic with copper in producing copper-enriched precipitates that evolve first as non-random fluctuations to embryos to clusters and then to precipitates. However, the situation is very complex, and there is also an important effect of Mn (and possibly Si) coupled with Ni, even for low Cu steels. When there is very little Mn, even for very high Ni content steels, very little embrittlement occurs. Thus, high Ni, when not combined with Cu and moderate Mn, is not a serious embrittling agent.

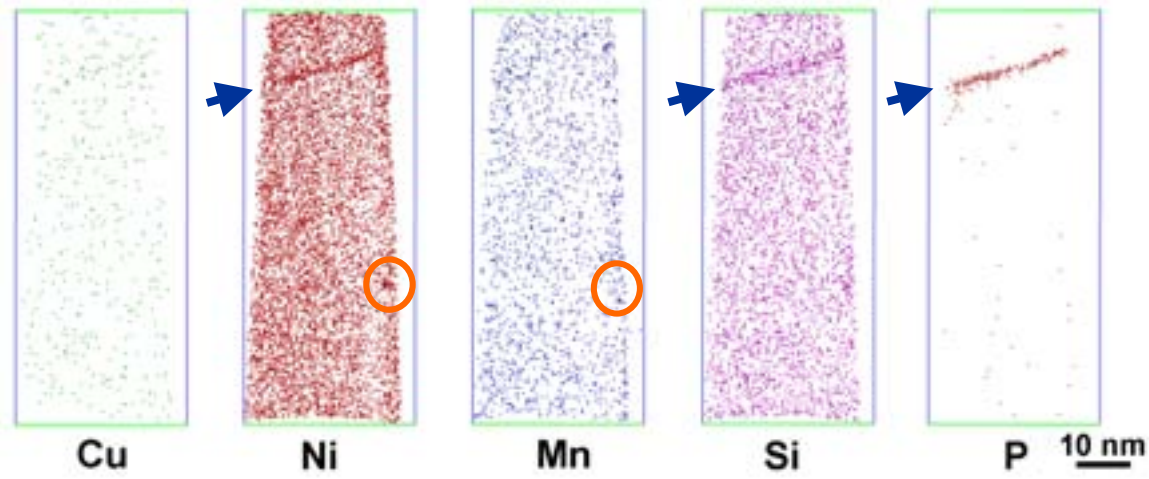

Fig. 6.1. Atom map from APT analysis of the WWER-1000 forging steel.

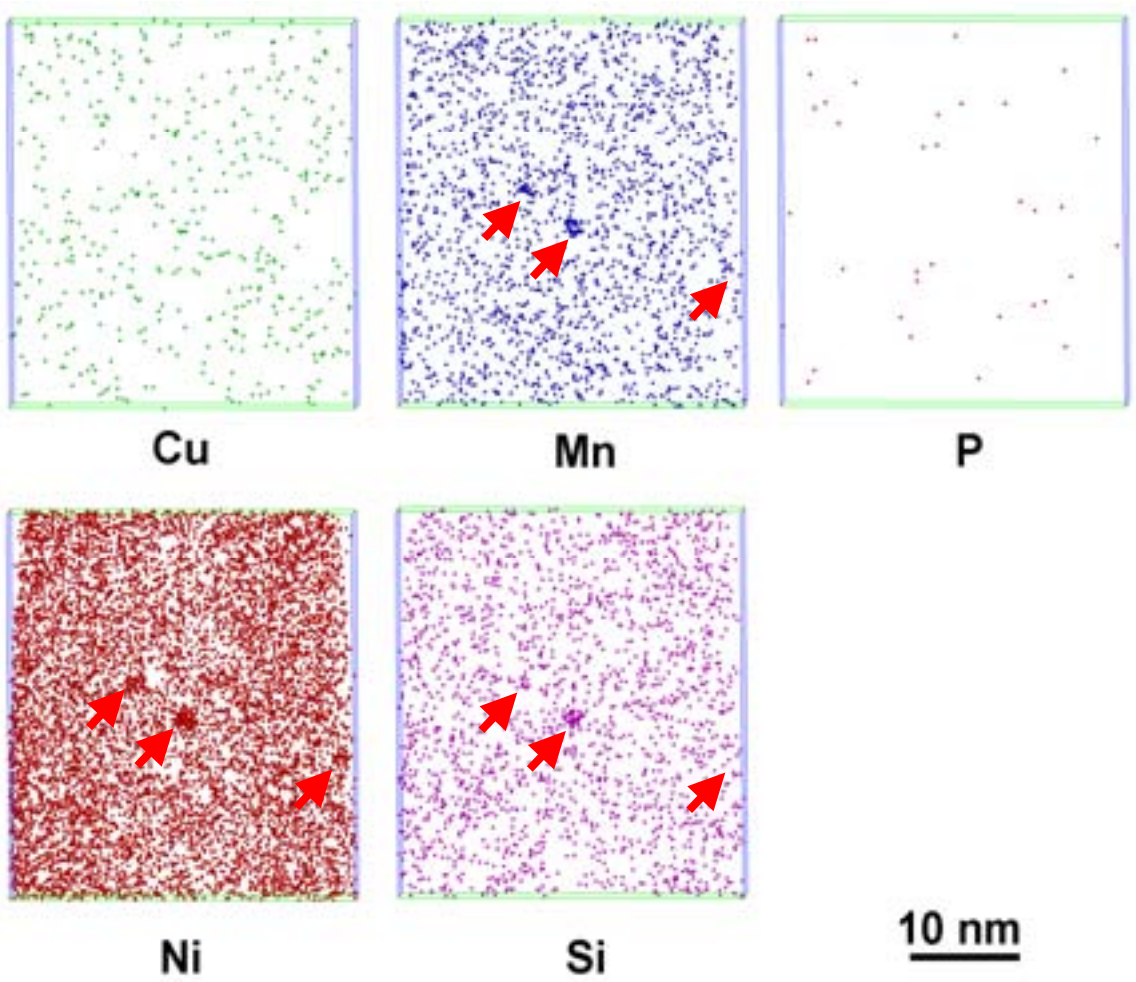

Fig. 6.2. Atom map from APT analysis of the WWER-1000 weld metal.

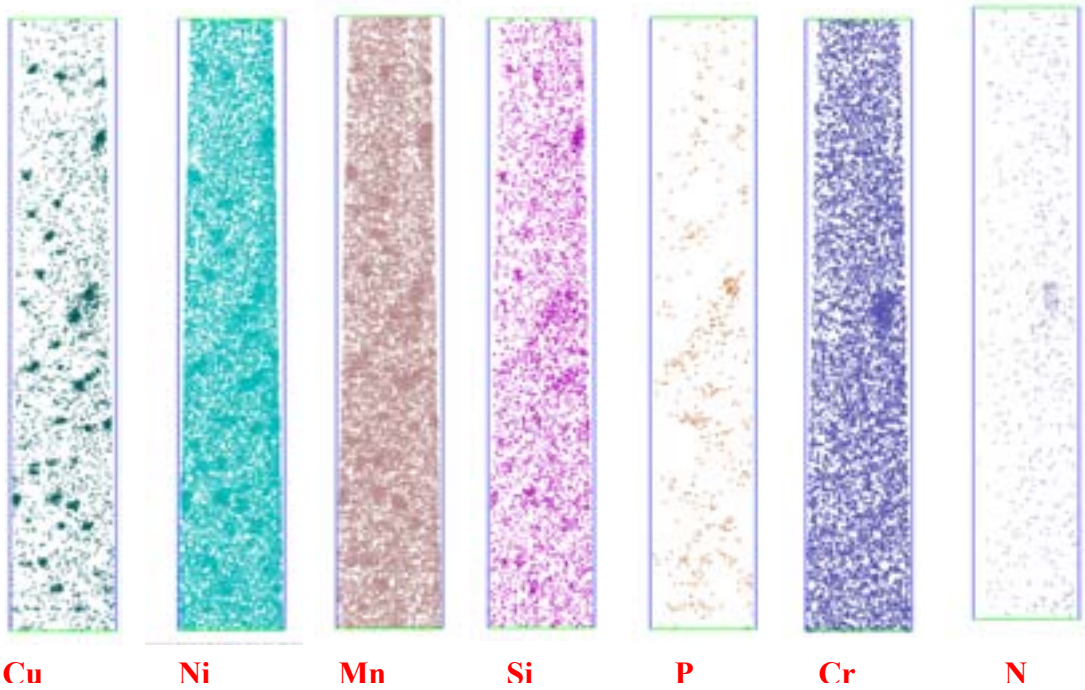

Fig. 6.3. Atom maps of the irradiated high-copper, high-nickel KS-01 submerged-arc weld reveal that irradiation produced an extremely high number density of precipitates, significantly higher than other RPV steels irradiated to similar or higher fluences. (note: Each dot is an atom. The box is 19 x 19 x 110 nm and contains 1.5M ions.).

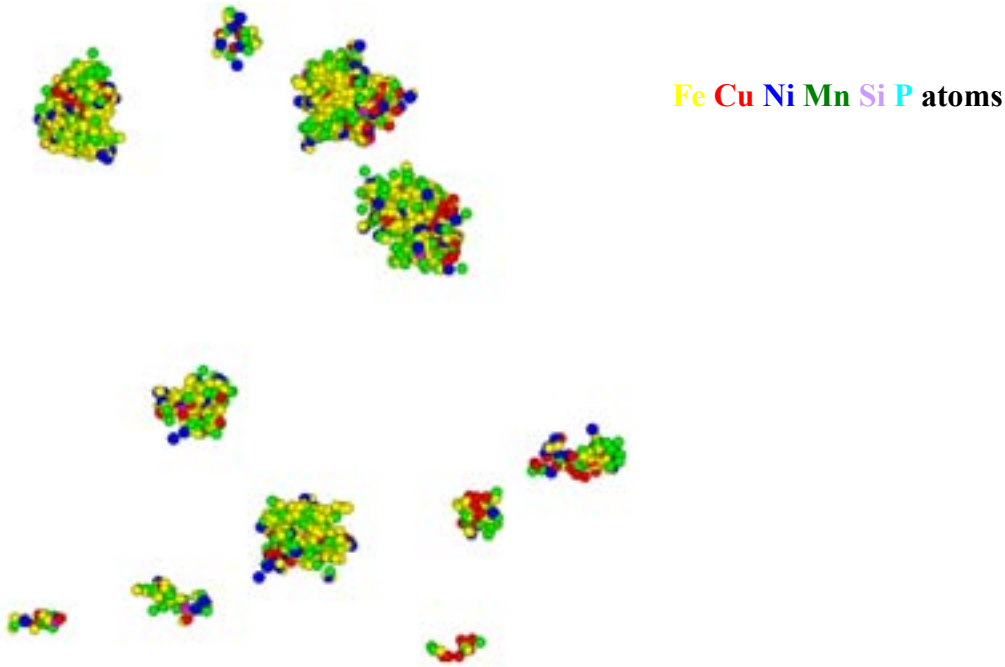

Fig. 6.4. Atom probe tomography images of the irradiated high-copper, high-nickel KS-01 submerged-arc weld show the approximately spherical morphology of copper-enriched precipitates.

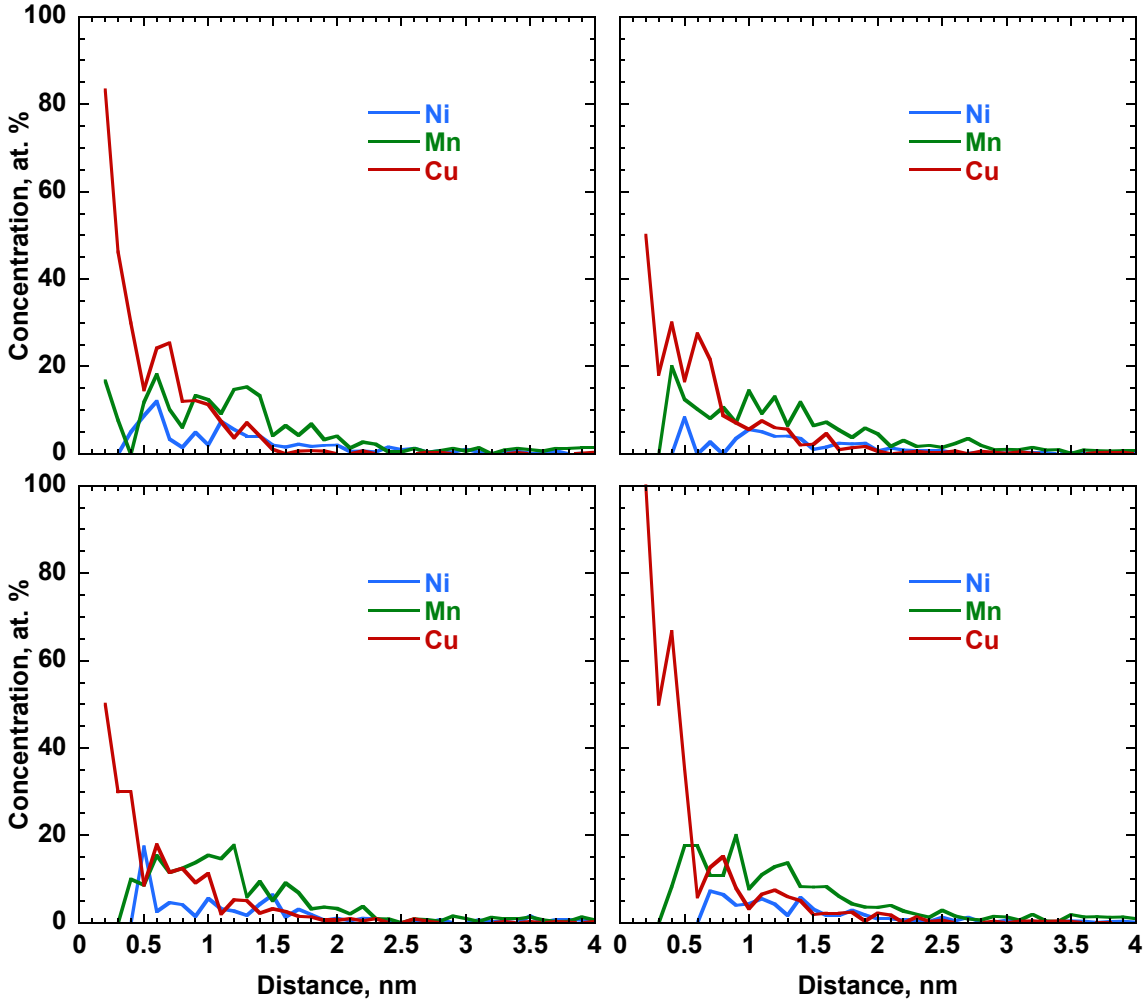

Fig. 6.5. APT data analysis provides the elemental concentration distribution relative to the precipitate center and shows that copper is concentrated at the core of the precipitate, that manganese has a more extensive profile into the matrix, and nickel is more associated with the interface.

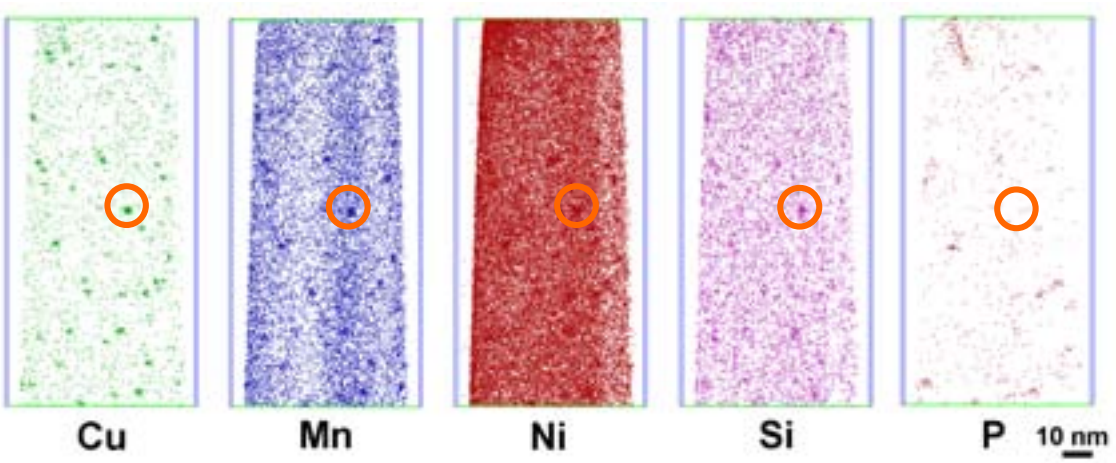

Fig. 6.6. Atom map from APT analysis of high Cu content A533B weld metal showing a high number density of Cu-, Mn-, Ni-, Si- and P-enriched precipitates.

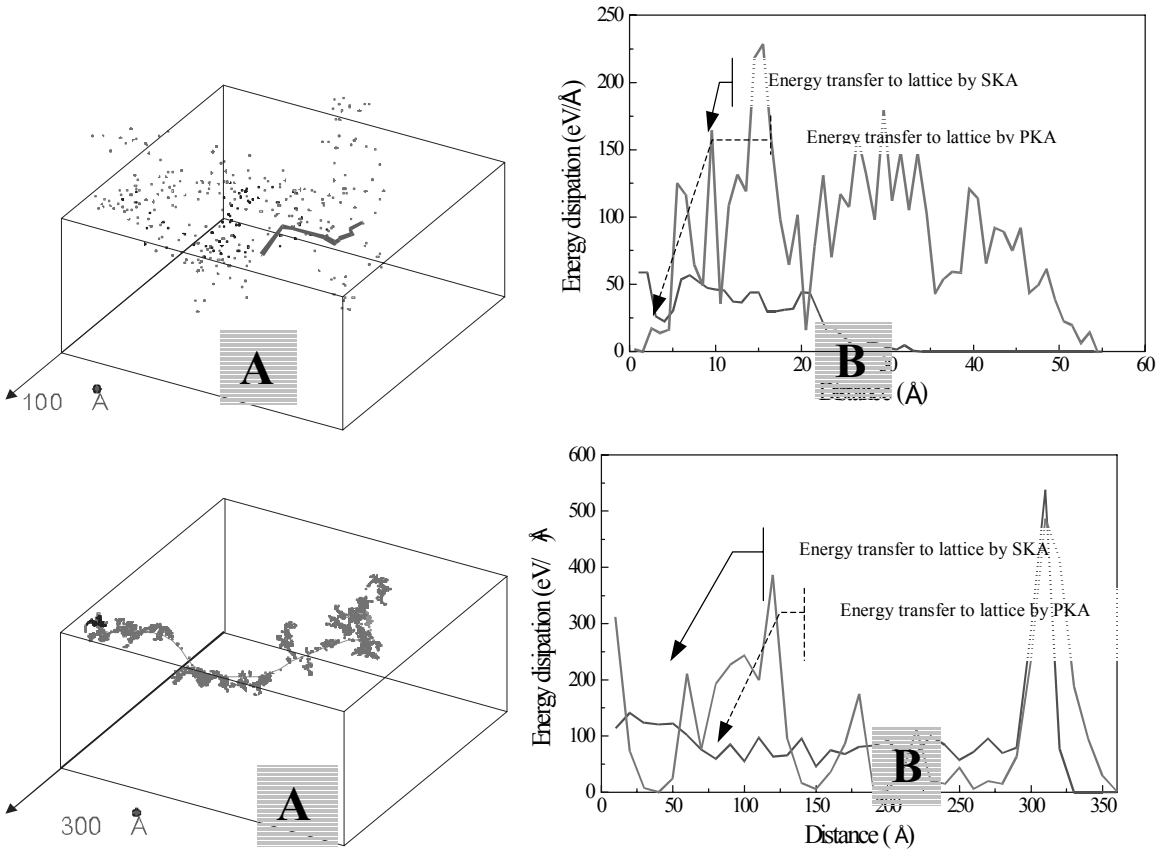

Fig. 6.7. Distribution of radiation defect in cluster (left panel) and energy transfer to the lattice (right panel) in an idealized metallic alloy for primary knock-on atom of 15keV (A) and 150keV (B).

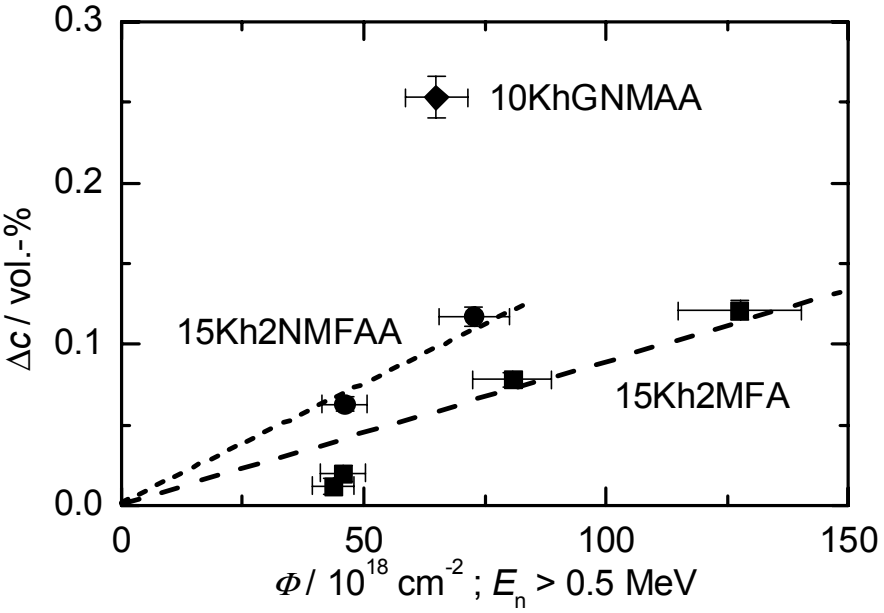

Fig. 6.8. Dose-characteristic, irradiation-induced non-ferromagnetic defect cluster content, Δc, measured by SANS versus neutron dose (dpa) of WWER-440 base metal 15Kh2MFA (0.1–0.3 wt. % Ni), WWER 1000 base metal 15Kh2NMFAA (1.1–1.3 wt. % Ni), and WWER 1000 weld metal 10KhGNMAA (1.7 wt. % Ni). Irradiation temperature for all three cases was 255°C.

REFERENCES

[6.1] KRYUKOV, A.M., NIKOLAEV, Y.A. AND NIKOLAEVA, A.V., in Nuclear Engineering and Design, 186, (1998) 353.

[6.2] WILLIAMS, T.J., BURTZ, P.R., ENGLISH, C.A. AND DE LA COUR RAY, P.H.N., 3rd International Symposium on Environmental Degradation of Materials in Nuclear Power Systems—Water Reactors, 1987, eds., G.J. Theus and J.R. Weeks, (1988) 121.

[6.3] Odette, R. and Lucas, G.E., *Irradiation Embrittlement of Reactor Pressure Vessel Steels: An International Review: ASTM STP 909***,** ed. L.E. Steele, American Society For Testing And Materials, (1986) 206.

[6.4] DEBARBARIS, L., ET AL., "Irradiation Embrittlement of Model Alloys and Commercial Steels; Analysis of Similitude Behaviours," *IAEA Specialists Meeting*, (Proc. Mtg. Gloucester, UK, 2002) International Atomic Energy Agency, Vienna, (2002).

[6.5] SERVER, W., ENGLISH, C., NAIMAN, D. AND ROSINSKI, S., "Charpy Embrittlement Correlations — Status of Combined Mechanistic and Statistical Bases for U.S. Pressure Vessel Steels (MRP-45)", Electric Power Research Institute 1000705, Palo Alto, CA, USA (2001).

[6.6] JAPANESE ELECTRIC ASSOCIATION CODE, 4201–2000, "Method of Surveillance Tests for Structural Materials of Nuclear Reactors," JEAC (2000).

[6.7] ELECTRIC POWER RESEARCH INSTITUTE, R.J. STOFANAK, ET AL., *EPRI Workshop on Dose Rate Effects*, Palo Alto, CA, USA (2001).

[6.8] AMERICAN SOCIETY FOR TESTING AND MATERIALS, M.G. BURKE, ET AL., "Microstructural Aspects of Irradiation Damage in A508 Gr 4N Forging Steel: Composition and Flux Effects," *The Effects of Radiation on Materials: 21st International Symposium, ASTM STP 1447*, ed., M.L. Grossbeck, (2003).

[6.9] UlBRICHT, ET. Al., Microstructural Investigations on Russian Reactor Pressure Vessel Steels by Small-Angle Neutron Scattering," Appl. Phys. A74 (Suppl.), S1128–S1130 (2002)

7. SUMMARY AND DISCUSSION

As stated in the introduction to this report, it is generally accepted that the presence of nickel in RPV steels increases its sensitivity to neutron induced embrittlement even at low phosphorus and copper concentrations. Additionally, it was stated that there is only a limited quantity of data on neutron embrittlement of WWER-1000 steels (Ni-Cr-Mo-V) with high nickel content (>1.5 wt%). As a result, the IAEA organized this CRP with the stated goal: "to provide information based on the results obtained that will allow for improved understanding of the effects of nickel on light-water RPV embrittlement that will lead to the development of improved predictive techniques."

Eleven institutes from eight different countries and the European Union participated, with irradiations being conducted by six of the institutes. One of the results from the testing on this CRP is the wide scatter observed in the unirradiated ductile-brittle transition temperature, $T_{41J\text{-}UN}$, for the WWER-1000 base metal (a forging). Although previous test results for similar forgings have shown greater scatter for base metal than for weld metals, the scatter from the present forging seems unusually high. As stated earlier, all specimens were machined by the same institute as one step in minimizing such variability. Because the material is known to exhibit relatively large scatter, then, it is difficult to determine the variability from testing in eight different laboratories. In this regard, however, inspection of the test results for the weld metal shows relatively low scatter in the $T_{41J\text{-}UN}$, implying that laboratory variability was not necessarily the primary factor in the scatter observed for the forging. This high scatter in the $T_{41J\text{-}UN}$ results is undoubtedly a key factor in the high scatter also observed in the irradiation-induced ΔT_{41J} values. Although irradiation temperatures varied among the participants experiments, inspection of those differences did not reveal the potential for changes that would substantially alter the relationships among the ΔT_{41J} values.

To attempt an accommodation of the scatter in the irradiated results, the mean $T_{41J\text{-}UN}$ from all unirrradiated tests ($T_{41J\text{-}ADJ}$) was used to recalculate $\Delta T_{41J\text{-}ADJ}$ values using the irradiated $T_{41J\text{-}IRR}$ result from each participant. This procedure resulted in a significant change in the plot of shift vs fluence for the base metal, but did not substantially change that for the weld metal.

In spite of the uncertainties resulting from the high scatter in the data, the results are clear in showing the significantly higher radiation sensitivity of the high nickel weld metal (1.7 wt%) compared with the lower nickel base metal (1.2 wt%). This result is supported by other similar results in the literature for WWER-1000 RPV steels, including those from research and commercial reactor experiments as well as from surveillance programs. Since the beginning of this CRP, substantially more surveillance data for WWER-1000 RPVs has become available.

The results provided in the CRP for national steels, as discussed in Chapter 5, demonstrate these observations. Additionally, Chapter 5 presents results of model alloys showing the significant effects of nickel on irradiation-induced embrittlement. Moreover, the results shown for PWR type RPV steels in this CRP have also shown the sensitizing effects of nickel on embrittlement. For example, Chapter 5 presents PWR data showing significantly higher irradiation-induced embrittlement for a weld with 1.7 wt% nickel compared to that for one with 1.0 wt%. Thus, the results are reflective of the predictive formulas for the PWR type

steels, which contain nickel content as a primary variable. However, the predictive formula for WWER-1000 RPV materials does not include nickel content as a variable.

The synergistic effects of manganese were mentioned in Chapter 5 which also includes data from national steels testing demonstrating that, for a given high level of nickel in the material and all other factors being equal, high manganese content leads to much greater embrittlement than low manganese content. Direct evidence of this effect, although postulated some years earlier, is relatively recent. In addition to the effect of manganese on the WWER-1000 steels, Chapter 5 also discusses results with national steels containing nickel content as high as 3.5 wt%, about two times higher than the WWER-1000 weld metal used for this CRP. This study showed that a superclean steel with high nickel (3.4 wt%), but with only 0.02 wt% manganese and 0.03 wt% copper, demonstrated quite low radiation sensitivity.

Although the fact that nickel is a significant factor in the radiation sensitivity of RPV steels has been known for a long time, the mechanisms for such effects have been more difficult to ascertain. Of course, this is because these mechanistic effects occur at the nano-scale in the microstructure. Four of the CRP participants performed microstructural investigations, including optical microscopy, scanning electron fractography, transmission electron microscopy, small-angle neutron scattering, positron annihilation, Mossbauer spectroscopy, 3-dimensional atom probe field ion microscopy, and atom probe tomography. Details of the investigations are discussed in Chapter 6.

However, it is clear from the various studies that nickel associates with copper in the irradiation-induced copper-enriched precipitates, and that manganese (and possibly silicon) is similarly associated. At least for the very high nickel steels examined (A508 grade 4N), an important observation is that when there is very little manganese, even for very high nickel content, very little irradiation-induced embrittlement occurs. Thus, at least for that steel, it appears that high nickel content, when not combined with copper and moderate manganese, is not a serious embrittling agent. For WWER-1000 steels with very low copper contents and irradiated to relatively low fluence, atom probe tomography has shown ultra-fine manganese-nickel-silicon enriched precipitates. Atom probe tomography of such steels at relatively high fluences has not been performed, but the results at low fluence compel the need for such examination.

8. CONCLUSIONS AND RECOMMENDATIONS

Eleven institutes from eight different countries and the European Union participated in this CRP, with irradiation experiments of the CRP WWER-1000 RPV materials being conducted by six of the institutes. In addition to the irradiation and testing of those materials, irradiation experiments of various national steels were also conducted. Moreover, some institutes performed microstructural investigations of both the CRP materials and national steels. This TECDOC presents and discusses all the results obtained and analyses performed within the CRP. The main conclusions are as follows:

1. The CRP WWER-1000 base metal Charpy test results exhibited significantly greater scatter in the unirradiated condition than those for the CRP WWER-1000 weld metal. The high scatter obtained with the base metal was determined to be due primarily to material variability and not laboratory-to-laboratory bias.

2. The analyzed results are clear in showing the significantly higher radiation sensitivity of the high nickel weld metal (1.7 wt%) compared with the lower nickel base metal (1.2 wt%). These results are supported by other similar results in the literature for both WWER-1000 RPV materials, PWR-type materials, and model alloys.

3. Regardless of the increased sensitivity of the CRP WWER-1000 high nickel weld metal (1.7 wt%), the transition temperature shift at the WWER-1000 RPV design fluence is still below the predicted curve from the Russian Guide. For higher fluences, no data were available and the results should not be extrapolated.

4. Although manganese content was not incorporated directly in this CRP, results from tests of national steels demonstrated that, for a given high level of nickel in the material and all other factors being equal, high manganese content leads to much greater irradiation-induced embrittlement than low manganese content for both WWER-1000 and PWR materials.

5. Microstructural investigations, including transmission electron microscopy, positron annihilation, and atom probe tomography, have shown, for both WWER-1000 and PWR materials, that nickel associates with copper in the irradiation-induced copper-enriched precipitates, and that manganese and silicon are similarly associated.

6. Experimental results and microstructural investigations for a very high nickel steel (~3.5 wt%) have indicated that, when there is very little manganese, the radiation sensitivity is very low even for such a high nickel steel.

The following recommendations are provided:

1. It is desirable to study the synergistic effect of nickel with manganese, respectively silicon to explain/understand the embrittlement mechanism of high/low nickel RPV steels/welds.

2. Detailed studies of changes in mechanical properties should be accompanied by microstructural investigations to be able to explain potential damage mechanisms and synergisms (qualitatively and even semi-quantitatively).

3. Regarding the potential synergistic effect of manganese and nickel to radiation embrittlement of WWER-1000 RPV materials and the fact that the predictive formula in the Russian Guide was evaluated on the basis of moderate nickel content (up to 1.5 wt.%), an activity for the revision of this formula is recommended.

LIST OF PARTICIPANTS' FINAL CRP REPORTS

CHATTERJEE, S., — Mechanisms of Nickel Effect in Radiation Embrittlement of Reactor Pressure Vessel Materials, Progress Report, Bhabha Atomic Research Centre, Trombay, India, December 2002.

GERASHCHENKO, S., — Investigation of Nickel Influence on the Radiation Embrittlement of WWER Reactor Pressure Vessel Materials; Final Report, Russian Research Centre „Kurchatov Institute", Moscow, Russian Federation, Otober 2003.

GRYNIK, E., — Investigation of the specimens of the materials of WWER-1000-type reactor pressure vessel with different content of nickel, National Academy of Sciences of Ukraine, Institute for Nuclear Research, Kiev, Ukraine, May 2003.

KAMENOVA, T., — Mechanicm of Ni Effect in Irradiation Embrittlement of Reactor Pressure Vessel Materials, Final Report, Institute of Metal Science, Sofia, Bulgaria; April 2003.

LIPKA, J., ET AL. — Nickel effect in radiation embrittlement of reactor pressure vessel steels studied by MS and PAS; Slovak University of Technology in Bratislava, Slolvak Republic, October 2002.

MOROZOV, A. NIKOLAEV, V., YURCHENK, E.,— Investigation of Nickel Effect on Radiation Embrittlement of Reactor Pressure Vessel Material. Radiation Embrittlement of WWER-1000 Pressure Vessel Material; Report; Central Research Institute of Structural Materials "Prometey", Saint-Petersburg, Russian Federation, 2003.

NANSTAD, R.K., SOKOLOV, M.A., MILLER, M.K., — Comparison of Effects of Nickel on Embrittlement Mechanisms in Prototype VVER-1000 Weld Metal and A533B Steel; Oak Ridge National Laboratory, Oak Ridge, TN, USA, March 2004.

NOVOSAD, P., FALCNIK, M., KYTKA, M. MALEK, J., BRUMOVSKY, M., — Irradiation and Mechanical Properties of the 15Kh2NMFAA and 12Kh2N2MAA Material with High Content of Ni, Final Report, Nuclear Research Institute Rez plc, Czech Republic, December 2003.

SERVER, W.L., — Micro-Mechanistic Understanding of Enhanced Embrittlement Due to High Levels of Nickel in RPV Steels, ATI Consulating, Pinehurst, NC, USA, February 2004.

URI, G., GILLEMOT, F., HORVATH, M., SIMONITS, A., — Mechanism of Nickel Effect in Radiation Embrittlement of RPV Materials; Research Report, KFKI Atomic Energy Research Institute, Budapest, Hungary, December 2002.

CONTRIBUTORS TO DRAFTING AND REVIEW

Brumovsky, M.	NRI Rez plc., Rez, Czech Republic
Debarberis, L.	JRC-IE, Petten, Netherlands
Kang, K.	International Atomic Energy Agency
Kryukov, A.	RRC Kurchatov Institute, Moscow, Russian Federation
Server, W.	ATI Consulting, USA
Nanstad, R.	Oak Ridge National Laboratory, USA

Research Coordinated Meetings

10–12 April 2000, Vienna, Austria
29–31May 2001, Sazopol, Bulgaria
2–4 December 2002, Pamporovo, Bulgaria

Consultants Meetings

Vienna, Austria:15–17 March 2004, 8–20 October 2004